FEDERAL UNIVERSITY OF PARÁ

GEOSCIENCES INSTITUTE

POST-GRADUATE PROGRAM IN GEOPHYSICS

Master 's Dissertation

Tying seismic to well based on deterministic wavelet estimative and predictive deconvolution: application in the North Sea seismic/well data

ISADORA AUGUSTA SANTANA DE MACEDO

Belém-Pará

2015

ISADORA AUGUSTA SANTANA DE MACEDO

Tying seismic to well based on deterministic wavelet estimative and predictive deconvolution: application in the North Sea seismic/well data

Master's dissertation submitted to the Post-Graduate Program in Geophysics from the Geosciences Institute at Federal University of Pará for the obtainment of the title of Master in Geophysics

Orientador: Carolina Barros da Silva
Coorientador: José Jadsom Sampaio de Figueiredo

Belém-Pará

2015

TYING SEISMIC TO WELL BASED ON DETERMINISTIC AND PREDICTIVE DECONVOLUTION: APPLICATION IN THE NORTH SEA SEISMIC/WELL DATA

ISADORA AUGUSTA SANTANA DE MACEDO

Master's thesis submitted to the Post-Graduate Program in Geophysics from Geosciences Institute at Federal University of Pará for the obtainment of the title of Master in Geophysics

Approval Date : 04 / 12 / 2015
Grade: 9,0 (EXC)
Committee Members:

_____
Prof. Carolina Barros da Silva (Adviser)
Ph. D. in Geophysics
Federal University of Pará – UFPA
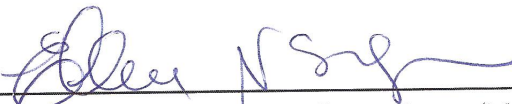
_____
Prof. Ellen de Nazaré Souza Gomes (Member)
Ph. D. in Geophysics
Federal University of Pará – UFPA

_____
Prof. Daniel Leal Macedo (Member)
Ph. D. in Science and Petroleum Engineering
University of Campinas

Ao Zé Macedo, Deolinda e Bernardo.

ACKNOWLEDGMENTS

RESUMO

A estimativa da wavelet, assim como a amarração poço-sísmica, são procedimentos importantes no processamento e na interpretação sísmica. Neste trabalho é desenvolvido um estudo comparativo de amarração dos dados de poço aos dados sísmicos. A comparação reside nas diferentes maneiras abordadas para realizar a estimativa da wavelet: uma abordagem determinística, baseada tanto nos dados sísmicos quanto nos dados de poço e uma abordagem estatística, baseada na deconvolução preditiva e nas suposições clássicas do modelo convolucional da Terra. Os testes com dados numéricos mostram a estimativa da wavelet com uma certa precisão em ambos os casos. A viabilidade desta abordagem é também verificada nos dados reais de sísmica e poço provenientes do Viking Graben, no Mar do Norte na Noruega. Os resultados também mostram a influência das zonas lavadas do poço na qualidade da amarração poço-sísmica.

Palavras-chave: Deconvolução preditiva. Amarração poço-sísmica. Estimativa da wavelet. Mar do Norte

ABSTRACT

Wavelet estimation as well as well-tie procedure are important tasks in seismic processing and interpretation. In this work we perform comparative study of the well-to-seismic tie. The comparison relies on different approaches to estimate the wavelet: a deterministic estimation, based on both seismic and well log data, and a statistical estimation, based on predictive deconvolution and the classical assumptions concerning the convolutional model. Tests with numerical data show the estimation of seismic wavelet with reasonable accuracy for both cases. The feasibility of this approach is also verified on the real seismic and well data from Viking Graben field, North Sea, Norway. The results also shown the influence of the washout zones on the well log data on the well to seismic tie.

Keywords: Predictive deconvolution. Well tie. Wavelet estimation. North Sea.

LIST OF ILLUSTRATIONS

SUMMARY

1 INTRODUCTION

The earth is composed of rock's layers with different lithology and physical properties. By the seismic point of view, these layers are represented as the densities and velocities with which seismic waves propagates through them. The product of density by velocity is the seismic impedance and it is the impedance contrast between adjacent rock layers that causes the reflections that are recorded along a surface profile. These signnals compose the real seismic data. The recorded seismogram can also be modeled as a convolution of the earth's reflectivity with the seismic wavelet. This wavelet has many components, including source signature, recording filter, surface reflections and receiver-array response (YILMAZ, 2000).

Well-tie is an useful tool to relate recorded seismic waveforms to the stratigraphy and rock properties of the subsurface (WHITE; SIMM; XU, 1998). Accurate well-tie are essential to practical seismic lithological interpretation (WHITE, 2003). As long as the geology in the vicinity of the well is not unduly complex, the main factors controlling this accuracy are the processing of the seismic data and the construction of the seismic model from the well logs. The main link between a primary reflection signal and the reflectivity constructed from a well log is the seismic wavelet. In general, most of the studies on this subject states that methods to estimate the seismic wavelet are divided in two categories: deterministic and statistical. Deterministic methods require direct measurements of the source wavefield or the use of the well log data (OLDENBURG; LEVY; WHITTALL, 1981; YILMAZ, 2000). Statistical methods estimate the wavelet from the seismic trace itself and require assumptions about the characteristics of the wavelet (BULAND; OMRE, 2003; LUNDSGAARD; KLEMM; CHERRETT, 2015). This last, is based on mathematical tools to solve the problem of wavelet estimative.

The possibilities to solve the seismic wavelet estimative problem are enormous and the complexity of the methods just increase with time. White e O'brien (1974) analyzed three methods to obtain the phase spectrum of the wavelet. The first was the method of the Hilbert Transformation or Kolmogorov method (KING, 2010), which is based on the assumption that the wavelet is minimum phase. This means that the phase spectrum can be calculated from the Hilbert transformation of the logarithm of the amplitude spectrum of the wavelet. The second uses the Z transform and the third involves spiking deconvolution. The Hilbert Transformation method is from the works of Robinson (1957) and Robinson (1967).

White (1980), White (2003) proposed the Well-Tie Matching (WTM) technique, where the wavelet is estimated directly from the seismic data through a least squares technique, treating the well-tie as a noisy input-noisy output problem. In this approach,

several parameters are used to diagnose the quality of the tie, such as the proportion of trace energy predicted (PEP) by the synthetic seismogram, a measure of the goodness of fit and the normalized mean square error (NMSE), a measure of the accuracy of the tie. This study followed the tutorial of good practice in well ties made by the same authors White (2003), although the procedure to estimate the wavelet adopted in this work was different.

Edgar e Baan (2011) tested statistical methods to estimate the wavelet against the deterministic method. The statistical methods were based on the estimative of the phase using a consequence of the Central Limit Theorem. Which states that a convolution of any filter with a white time series yields the amplitude distribution of the output nearly to Gaussian behaviour. The wavelet phase is found by phase rotating the seismic data until the amplitude distribution becomes maximally non-Gaussian.

In this study we compare the quality of the well to seismic tie based on two different methods to estimate the wavelet. The first one is the traditional deterministic method, which selects a segment of the reflection sequence and a segment of the seismic data. The best wavelet estimated is the one that leads to the best match between seismic and synthetic. It is worthy to mention that our statistical approach is based on predictive deconvolution and has a low computational cost. This deconvolution is based on the classical assumptions concerning the convolutional model of the earth. Our algorithms, for both wavelet estimatives, introduce an semi-automatic approach to tying seismic traces to wells that improves correlation among well ties.

It is important to clarify aspects related to the concepts of *statistic* and *deterministic* in this work. There are two point of views when using those two concepts. From the point of view of the solution of the deconvolution problems, *deterministic* means that the source signature is known (as will be discussed on 2). In this case, no wavelet need to be estimated as it is already known. From the same point of view, *statistic* means that the source signature is unknown. In this case it is necessary to introduce new assumptions about the convolutional model to solve the problem of the deconvolution and, consequently, estimate the seismic wavelet.

On the other hand, from the point of view of the methods to estimate the seismic wavelet for the well to seismic tie, it can be divided in two categories. The categorie named *statistic* indicates that the input to the method to estimate the wavelet is only the seismic data, therefore, this method is based on mathematical tools to estimate the wavelet. The other categorie named *deterministic* is the one that uses both the seismic data and the well log data to estimate the seismic wavelet.

Tests with numerical data using our semi-automatic algorithm to estimate the wavelet show the estimation of seismic wavelet with reasonable accuracy for both statistical and deterministical cases. Besides, the feasibility of this approach is also verified on the

real seismic and well data from Viking Graben field, North Sea, Norway.

This work has a format of a paper. It will be necessary to reduce its size for submission. Its structure is as follows: chapter 2 adresses the theoretical background concerning the procedures to create the synthetic trace and estimate the seismic wavelet. As this work is based on the classical convolutional model, all its assumptions are explained as well as the deconvolution filters, with a special attention on the Wiener filter, once it is the one used to implement the predictive deconvolution to estimate the seismic wavelet. Chapter 3 shows the results of our semi-automatic implementation to do the well to seismic tie on a synthetic data. This step is important in order to have control of the accuracy of the algorithm. Chapter 4 shows the application of the same semi-automatic implementation on a real data set from the Viking Graben, North Sea. In this chapter it is shown the well to seismic tie made with a stacked and a migrated seismic section and information from two wells present on the Viking Graben data set. On chapter 5 a discussion is made about the results obtained with our algorithm on the real data set; moreover, a connection between the results and possible causes that affects the quality of the tie is made. Finally, chapter 6 expound the major conclusions that we obtained and suggestions to continue this work.

2 THEORETICAL BACKGROUND

All procedures to create a synthetic trace and to estimate the wavelet in this study was based on the classic convolutional model of the seismogram and its assumptions. Because of that, in this section a detail explanation about this model and a discussion about the assumptions are made. Besides that, the theory related to deconvolution, inverse filtering and the optimum Wiener filters is explained to have the necessary background to introduce the predictive deconvolution.

2.1 The Convolutional Model

The recorded seismogram $s(t)$ can be modeled as the convolution of the Earth's reflectivity $r(t)$ with the seismic wavelet $w(t)$ plus recorded noise $n(t)$:

$$s(t) = w(t) * r(t) + n(t). \tag{2.1}$$

According to Yilmaz (2000) several assumptions can be made for this convolutional model.

Assumption 1: The earth is made up of horizontally deposited layers of constant velocity.

Assumption 2: An impulsive seismic source generates a compressional pressure wave (P-wave) that interacts on layer boundaries have normal incidence. Therefore, no shear waves (S-waves) are generated.

The first assumption is violated in structurally complex areas, which a lateral velocity changes are present. The second assumption implies that this model for the seismic trace is based on a zero-offset recording scheme, an unrealizable experiment. Both of these assumptions suggests a normal incidence seismogram, where the reflection coefficient c, which is associated with the boundary between layers 1 and 2, is defined as:

$$R_c = \frac{\rho_2 v_2 - \rho_1 v_1}{\rho_2 v_2 + \rho_1 v_1}, \tag{2.2}$$

or in discrete representation,

$$R_c(i) = \frac{\rho_{i+1} v_{i+1} - \rho_i v_i}{\rho_{i+1} v_{i+1} + \rho_i v_i}. \tag{2.3}$$

The seismic impedance associated with each layer is given by the product ρv, where ρ and v are the densities and the velocities of the layers being considered. For this model, seismic amplitudes are related to acoustic impedance variations.

The pressure wave created by the impulsive source is called the signature of the source and it is described as a band limited wavelet of finite duration. As this wavelet travels through the earth, its amplitude decays because of wavefront divergence and frequency attenuation due absorption effects of rocks. This change of the wavelet with the time and depth is not incorporated on the convolutional model of the recorded seismogram, in other words, the convolutional model assumes that the wavelet is stationary, which yields the third assumption.

Assumption 3: The source wavelet is not dependent to the time or depth, it does not change as it travels in the subsurface - it is considered stationary.

The process of deconvolution seeks to unbuilt the convolution and recover the reflectivity from the recorded seismogram. The random noise present in the seismogram has several sources, such as wind motion, poorly coupled geophones and internal noise from the recording instruments. A pure random noise series has a white spectrum nearly flat. The autocorrelogram has a spike at zero lag and is nearly zero at all other lags. For all parameters that constitute the equation of the convolutional model, only the seismogram $s(t)$ is normally known. The earth's reflectivity needs to be estimated and the source wavelet is usually unknown although in some situations its signature can be measured. With three unknown factors $(w(t), r(t), n(t))$ and only one known $(s(t))$ in the proposed model, more assumptions needs to be performed.

Assumption 4: The noise component $n(t)$ is zero.

Assumption 5: The source waveform is known.

Under these new assumptions, the convolutional model is given by:

$$s(t) = w(t) * r(t). \tag{2.4}$$

If the wavelet is known (assumption 5), the solution of the deconvolution problem is deterministic. Therefore, equation 2.4 has a single unique solution for the reflectivity. If, however, the seismic wavelet is unknown, which is the usual case, the solution of the deconvolution problem is statistical and new assumptions needs to be made to solve the problem of the deconvolution.

As the convolution operation in the time domain is equivalent to a multiplication in the frequency domain, the amplitude spectra of the recorded seismogram is:

$$S(\omega) = W(\omega)R(\omega). \tag{2.5}$$

The overall shape of the amplitude spectra of the wavelet is close to the overall shape of the amplitude spectra of the recorded seismogram. They are not equal because the amplitude spectra of the reflectivity is not entirely random. However, if the reflectivity series were purely random, it would have a white spectrum, and the amplitude spectra of

the wavelet and the seismogram would be similar. In order to have more flexibility in the Assumption 5, a new assumption is made.

Assumption 6: The reflectivity is a random process. This implies that the seismogram has characteristics of the seismic wavelet in that their amplitude spectra and autocorrelations are similar.

The Assumption 6 guides the predictive deconvolution. It allows the autocorrelogram of the wavelet, which is unknown, to be replaced by the autocorrelogram of the seismogram, which is known, in the implementation of this deconvolution.

2.1.1 Inverse Filtering

Using all the assumptions above, the inverse filter $f(t)$ is an operator such that when convolved with the recorded seismogram $s(t)$, the output is the reflectivity series $r(t)$

$$r(t) = f(t) * s(t). \tag{2.6}$$

The convolutional model then becomes

$$s(t) = w(t) * f(t) * s(t). \tag{2.7}$$

When supressing $s(t)$ from both sides, the result is

$$\delta(t) = w(t) * f(t), \tag{2.8}$$

where $\delta(t)$ represents the Kronecker delta function. The filter operator $f(t)$ obtained is:

$$f(t) = \delta(t) * \frac{1}{w(t)}. \tag{2.9}$$

The inverse filter operator $f(t)$ needed to compute the earth's reflectivity from the recorded seismogram is mathematically the inverse of the seismic source wavelet $w(t)$. The inverse filtering is a form of deconvolution. As the seismic source wavelet needs to be known, this type of deconvolution is a method of deterministic deconvolution. And it can be improved by using the least squares minimization.

2.1.2 Least-Squares Inverse Filtering

The formulation of the deconvolution problem using the least-squares inverse filtering is as follows: given a input wavelet (c, d), the goal is to find the terms of a filter

(a, b) such that the error between the real output - convolution of the input wavelet and the filter $(ac, ad + bc, bd)$ - and the desired output (e, f, g) is the minimum. The sum of the squares of the differences between the coefficients of the real output and the desired output is measured by the cumulative energy of error L.

$$L = (ac - e)^2 + [(ad + bc) - f]^2 + (bd - g)^2. \tag{2.10}$$

The coefficients (a, b) need to be such that L takes its minimum value. If the desire output has an energy distribution that resembles on the real output and consequently, the error is reduced. A more generic formulation to compute the cumulative energy of error L of the least squares minimization is shown at the appendix A

2.1.3 Minimum Phase

The source wavelet is defined as a transient waveform with a finite duration. Assumption 3 states that in the convolutional model, the wavelet is stationary. But another assumption must be made about the wavelet regarding its phase. A wavelet can be zero, minimum, maximum or mixed phase. A maximum phase wavelet has most of its energy concentrated at the end of the time series; a mixed phase wavelet has its energy distributed throughout the time series; a minimum phase wavelet has its energy maximally concentrated at its onset. A zero phase wavelet is a modified wavelet (can be any of the ones previously mentioned) that have its maximum amplitude lying in the interface of two layers. These wavelets with different energy distribution can have the same amplitude spectra but have different phase-lag spectra. Moreover, the wavelet is physically defined - it has a finite time series - and is causal - it is zero for all negative times. In summary, a minimum phase wavelet is the one that is well defined, causal and has a minimum phase.

As the inverse filter coefficients are obtained by the inverse of the source wavelet, for this operation be stable, the filter coefficients need to make a convergent series, that is, they decrease with increasing time and tend to vanish at infinity; in other words, the filter has finite energy. Minimum phase wavelets have stable inverses but maximum and mixed phase wavelets do not. Therefore, the final assumption about the convolutional model is made

Assumption 7: The seismic wavelet is minimum phase and has a minimum phase inverse.

2.1.4 Optimum Wiener Filters

Determine the Wiener filter coefficients requires the solution of the normal equations:

$$\sum r_{i-\tau} a_\tau = g_i, \tag{2.11}$$

or in matrix terms

$$
\begin{pmatrix}
r_0 & r_1 & r_2 & \cdots & r_{n-1} \\
r_1 & r_0 & r_1 & \cdots & r_{n-2} \\
r_2 & r_1 & r_0 & \cdots & r_{n-3} \\
\vdots & \vdots & \vdots & \ddots & \vdots \\
r_{n-1} & r_{n-2} & r_{n-3} & \cdots & r_0
\end{pmatrix}
\begin{pmatrix}
a_0 \\ a_1 \\ a_2 \\ \vdots \\ a_{n-1}
\end{pmatrix}
=
\begin{pmatrix}
g_0 \\ g_1 \\ g_2 \\ \vdots \\ g_{n-1}
\end{pmatrix},
\tag{2.12}
$$

where r_i represents thet autocorrelation lags of the input wavelet, a_i, and g_i are the Wiener filter coefficients and crosscorrelation lags of the desired output with the input wavelet, $i = 0, 1, 2, ..., n - 1$, respectively. The autocorrelation matrix of the input wavelet is a symmetric Toeplitz matrix that can be solved by Levinson recursion. The demonstration of equation (2.12) is depicted in Appendix A.

The Wiener filter is optimum because the least squares error between the actual and desired output is minimum. Moreover, this filter can be used in a large class of problems once it is possible to considered any desired output, such as zero-lag spike (in that case, the Wiener filter is identical to the least-squares inverse filter and is called spiking deconvolution), spike at arbitrary lag, time-advanced form of input series, which configures the predictive deconvolution to be discussed later, zero-phase wavelet, or any desired arbitrary shape. To ensure numerical stability (prevent division by 0) when computing the inverse filter, an artificial level of white noise is added to the data before the deconvolution, process called pre-whitening. It can be added to the diagonal of the autocorrelation matrix.

2.1.4.1 Predictive Deconvolution

When the desired output on the normal equations is a time-advanced form of the input series, it suggests a prediction process. If a input series $x(t)$ is given and the goal is to predict its value at some future time $x(t + \alpha)$, where α is the prediction lag, it configures the predictive deconvolution. Wiener showed that the filter used to estimate $x(t + \alpha)$ is a special form of the general normal equations, and it is given by:

$$r_{\alpha+\tau} = \sum_t x_t x_{t-(\alpha+\tau)}, \tag{2.13}$$

or in matrix terms

$$
\begin{pmatrix}
r_0 & r_1 & r_2 & \cdots & r_{n-1} \\
r_1 & r_0 & r_1 & \cdots & r_{n-2} \\
r_2 & r_1 & r_0 & \cdots & r_{n-3} \\
\vdots & \vdots & \vdots & \ddots & \vdots \\
r_{n-1} & r_{n-2} & r_{n-3} & \cdots & r_0 \\
& , & & &
\end{pmatrix}
\begin{pmatrix}
a_0 \\
a_1 \\
a_2 \\
\vdots \\
a_{n-1}
\end{pmatrix}
=
\begin{pmatrix}
r_\alpha \\
r_{\alpha+1} \\
r_{\alpha+2} \\
\vdots \\
r_{\alpha+n-1}
\end{pmatrix} .
\tag{2.14}
$$

That is the case for a n-long prediction filter and a α-long prediction lag. The prediction filter requires only the autocorrelation of the input series. The demonstration of equation (2.14) is depicted in Appendix A.

Robinson (2008) explained how the predictive deconvolution works. The canonical representation of a seismic trace states that a nonminimum-delay trace can be represented by the convolution of an all-pass filter (which has a flat magnitude spectrum) and a minimum-delay wavelet. Both the trace and the wavelet have the same magnitude spectrum (the same color). It is well established that *white* refers to anything that has a flat magnitude spectrum, whereas *colored* refers to anything that has a curved or nonwhite magnitude spectrum. Thus, the trace model can be defined as:

1. Seismic trace = mixed-delay wavelet * reflectivity;

2. A mixed-delay wavelet has both a colored and a white component: mixed-delay wavelet = minimum-delay wavelet * all-pass wavelet;

3. It is possible to rewrite the seismic trace as: seismic trace = minimum-delay wavelet * (all-pass filter * reflectivity).

The convolution of the all-pass filter with the reflectivity composes the white components of the seismic trace. The process of predictive deconvolution separates on the basis of two criteria: "minimum-delay" and "white". Thus, it is important to relate the prediction process to the seismic trace to understand how the wavelet is estimated from this method. The prediction error filter (the error series of the predictive deconvolution) yields the white components of the seismic trace, that is the all-pass filter and the reflectivity. The prediction filter, the real output of the predictive deconvolution, yields the predictable components of the seismic trace, that is the "minimum-delay" component that constitute the minimum phase estimated wavelet.

Joining together the information concerning the inverse filtering, least squares inverse filtering and Wiener filter, it is possible to make several connections between the deconvolution filters. The inverse filtering transforms the wavelet directly into a spike, configuring a *spiking deconvolution* process. The least squares inverse filtering also

performs the spiking deconvolution but in a precisely manner. The Wiener filters can be design in a way that the input wavelet can be transformed in any desired output wavelet. Basically, the type of the deconvolution will depend on the desired output wavelet of the Wiener filter algorithm. If in the algorithm of the Wiener filter the desired output wavelet is set to be a spike with zero lag, it also configures a spiking deconvolution. If the desired output wavelet is set to be a spike with a arbitrary lag, it configures a spiking deconvolution with a arbitrary lag. In case the desired output wavelet is a time-advanced form of the input series, it is called *predictive deconvolution.* If the desired output of the deconvolution is any other form of wavelet, the process is called *wavelet shaping.*

2.2 Well to Seismic Tie

Well to seismic tie is a important part of interpreter's trade once they provide means of: 1) correctly identifying horizons to pick and 2) estimating the wavelet for inverting seismic data to impedance (WHITE; SIMM, 2013). It is a basic tool to analyze the connection of geology and seismic.

Borehole measurements such as sonic and density logs are recorded in depth while seismic measurements are in time. To convert the borehole measurements from depth to time, a time-depth relationship need to be established and the time-depth relationship at the borehole location is confirmed by generating a synthetic seismogram. In general, the creation of a synthetic include these steps:

1. Edit the sonic and density logs.

2. Generate a reflectivity series.

3. Apply a time-depth relationship.

4. Convolve the reflectivity series with a wavelet.

5. Compare the output of the convolution with the real seismic data.

The first step is necessary in order to not use noisy logs to generate the reflectivity series. Both the sonic and density curves have some spikes and null values that needs to be dealt with. The reflectivity series is generated by changes of impedance $I = \rho V_p$ within the earth. It is created directly from the sonic log and bulk density curves, according to the equation 2.3.

Since the sample rate of the well logs are larger than the sample rate of the seismic trace, the next step is to resample the reflectivity, so it can be fit on the time axis, from the time-depth relationship. With the reflectivity resampled on the time axis, it

can be convolved with a seismic wavelet to create a synthetic seismogram that will be further compared to the real seismic data. If there is a good set of logs, a wavelet that approximated of that one seismic section, and a good time-depth relationship, the tie between the seismic and the borehole should be good. The synthetic will be a "good match" to the seismic, with similar frequency content, high amplitudes in the same place and not much dispute from anyone who looks at the tie.

2.3   Semi-Automatic Algorithm to Estimate the Wavelet

In this section it is explained the implementation of the semi-automatic algorithm to perform the well to seismic tie used in this work. It performs a search for the best wavelet that produce the higher correlation coefficient between the synthetic trace and the real seismic trace. Figure 1 illustrates the procedure for the statistical and deterministic estimative of the wavelet.

Figure 1 – A schematic illustration of the algorithm for the estimative of the wavelet that produces the best well to seismic tie.
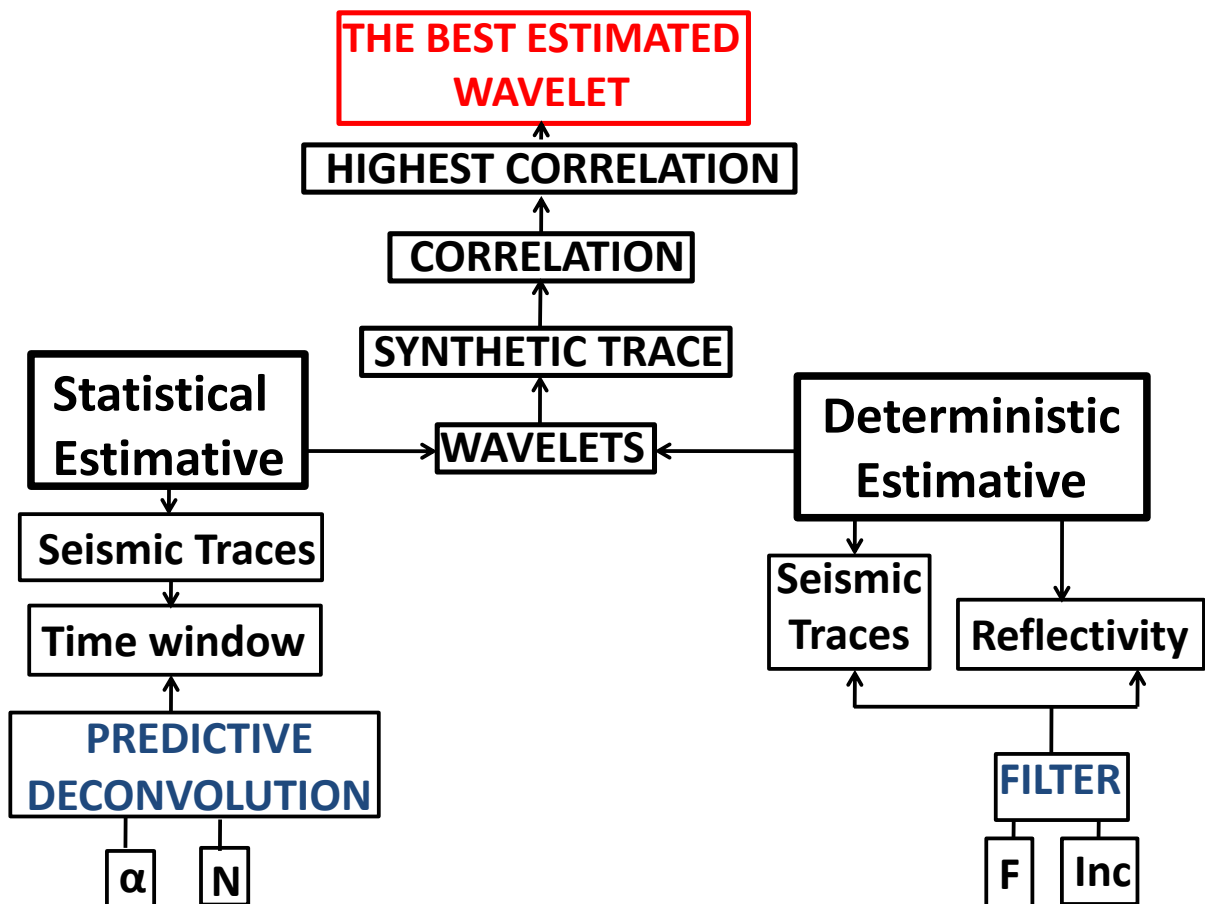
Source: From author.

The first step needed to estimate the wavelet through the predictive deconvolution

is select a range of traces in the vicinity of the well location (in stacking or migrated section). Then, on the segment chosen of each trace, a predictive deconvolution will be performed . The predictive deconvolution is dependent on the prediction lag (α) and the operator length (N). The choice of the best values of prediction lag and operator length produce the best result on the predictive deconvolution. For that reason, on the segment chosen, the predictive deconvolution is applied using a range of prediction lag and operator length. Each combination α-N generates a wavelet for all the range of CMPs that will be convolved with the reflectivity calculated from the wells. The correlation coefficient between the real seismic trace and all the synthetic traces generated with all the different wavelets are estimate. The algorithm identify the highest correlation coefficient and the trace (or corresponding CMP), the prediction lag and the operator length that yields it and generates the best statistical wavelet among all.

The other statistical alternative was to calculate the average wavelet. In this case, the procedure mentioned before is done with three or more different segments of the seismic trace. When the algorithm gives the best wavelet for each segment, an average wavelet is calculated. This average wavelet is the one that will be convolved with the reflectivity to generate the final synthetic seismic trace.

The left side of Figure 1 shows the well tie flow for the deterministic wavelet estimative. The inputs of the algorithm are the real seismic traces (from stacked or migrated section) in the vicinity of the well location and the reflectivity from the wells in a corresponding scale. In this case, a filter is built in a way that the convolution of the filter coefficients with the reflectivity, generates a synthetic trace that is as much as close to the real seismic trace as possible. This algorithm is dependent on the length of the filter (F) and the increment (Inc). This increment in time corresponds to the best match between the real trace and the synthetic trace. Each combination of filter length and increment generates a wavelet for all the range of traces. Each wavelet will be convolved with the reflectivity calculated from the wells and then the correlation between the synthetic and the real trace is performed. The algorithm identify the highest correlation coefficient and the trace, the filter length and the increment that generated it and produce the best deterministic wavelet among all.

The best wavelets calculated through the algorithms are the ones used to generate the synthetic traces of the well to seismic tie. The algorithm is not entirely automatic in the estimative of the best wavelet because on the statistical estimative, it is necessary to select a segment of the seismic trace in which the predictive deconvolution will be performed. It is recommended that this segment represents a reflectional signal from a interface so that the predictive deconvolution can separate the reflectivity component from the wavelet component. However, all the remain procedure to estimate the wavelet is automatic. As for the deterministic estimative, the process is semi automatic because the

seismic trace and the reflectivity in corresponding scales (the necessary inputs) are not made by the algorithm, it is made through the application of the time-depth relationship.

The advantages of this method is that several wavelets are generated and have the correlation coefficient tested and only the ones that produce the best match are selected. The implementation is not heavy and it is not computationally expensive. Even when using a large range of traces, prediction lag, operator length, filter length and increment, the processing time is very low.

3 APPLICATION ON SYNTHETIC DATA

In order to compare the feasibility of the well to seismic tie made with a wavelet estimated from a deterministic and statistical approaches, we test it first on a synthetic model. Our synthetic model consists of 6 layers and its logs are shown at Figure 2.

Figure 2 – P-wave, density and impedance logs related to a synthetic model with 6 layers.
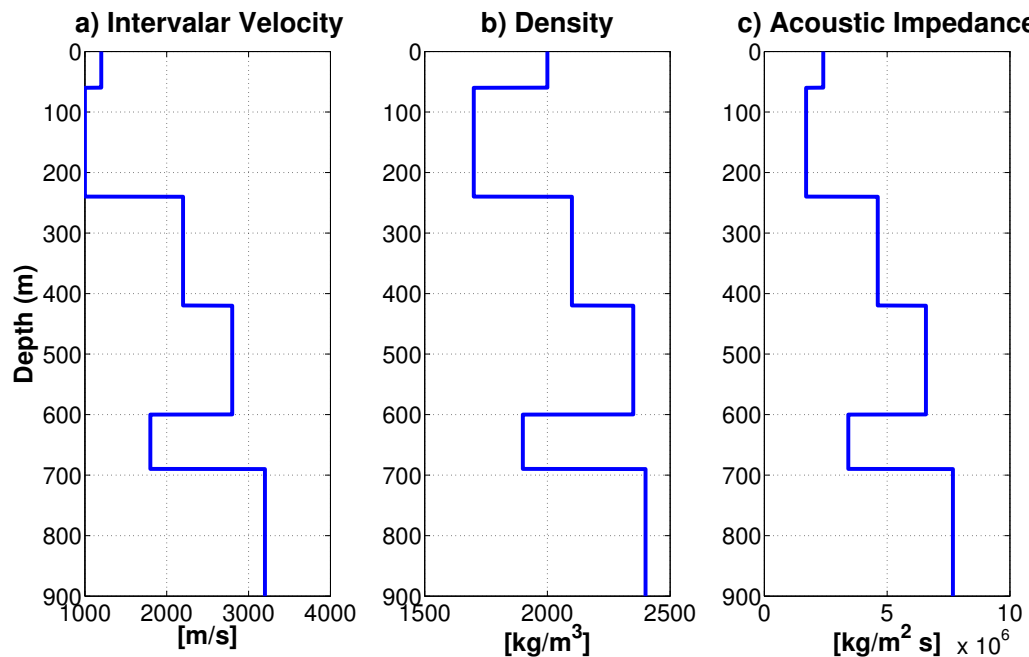
Source: From author.

The reflectivity was calculated according to equation 2.3 and then resample to accordingly fit the time axis, which has a total length of 3 s and a sample rate of 0.004 s. Figure 3 shows the corresponding reflectivity of model depicted at Figure 2.

The wavelet used to compute the synthetic trace was a Ricker pulse with a peak frequency of 20 Hz. The convolutional model states that the seismic trace can be modeled by the convolution of the reflectivity series with a wavelet. Two seismic traces were modeled, one with white noise and one without white noise. Figure 4 and Figure 5 shows the corresponding wavelets as well as the synthetic seismic trace without and with noise respectively.

We perform the least squares inverse filtering and the predictive deconvolution on the seismic trace in order to have a control of the algorithm when using the real data. Then, with the wavelet estimated from both methods, we created the synthetic trace and then compared to the real trace of the layer model.

Figure 3 – Reflectivity on depth domain created through the acoustic impedance and the reflectivity resampled to fit the time axis.
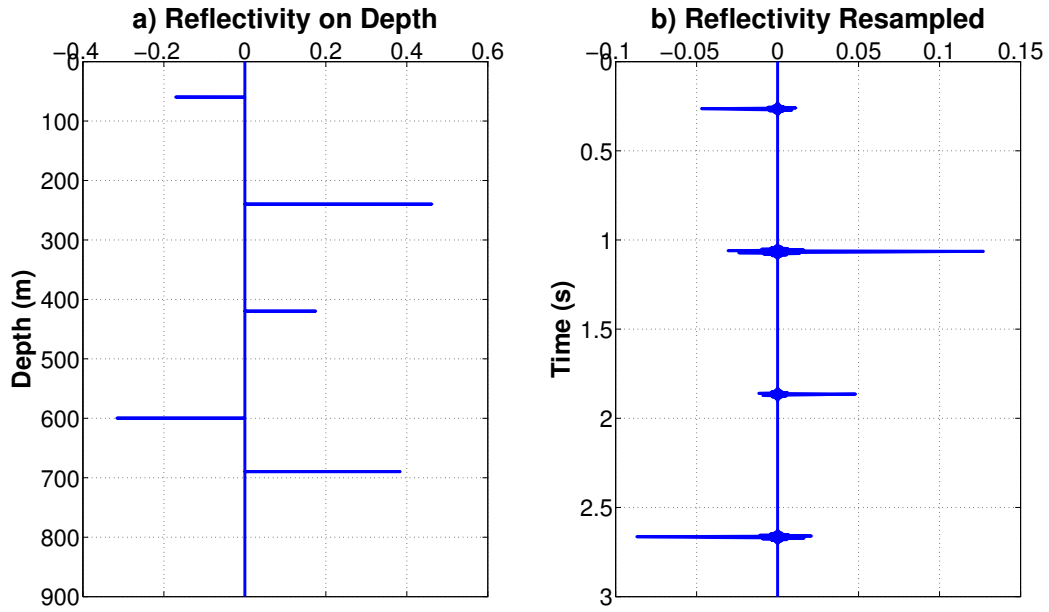
Source: From author.

Figure 4 – Seismic trace produced by the convolution of the reflectivity with the Ricker pulse.
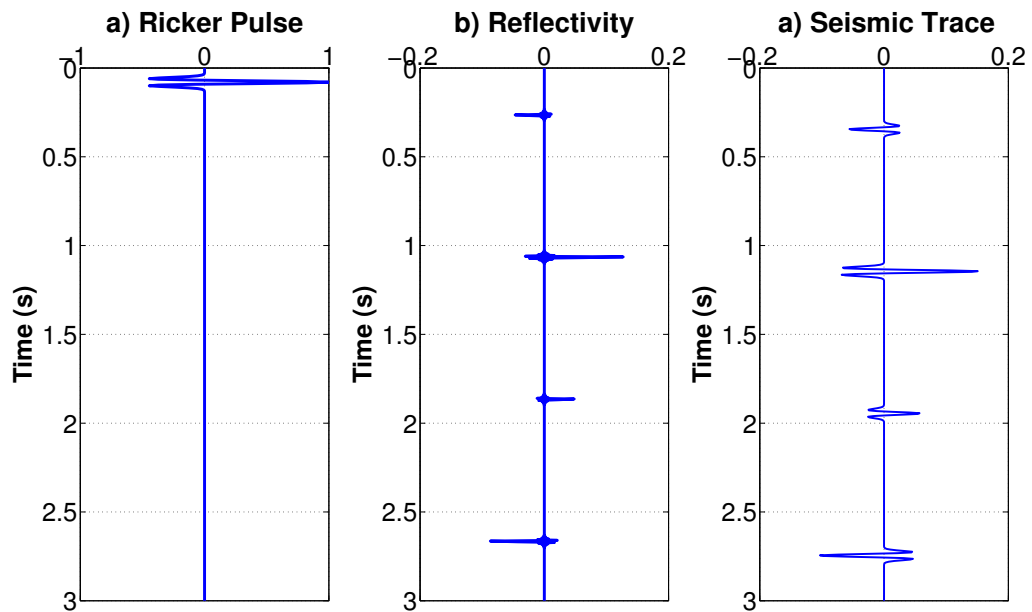
Source: From author.

Figure 5 – Seismic trace produced by the convolution of the reflectivity with the ricker pulse and the addition of white noise.
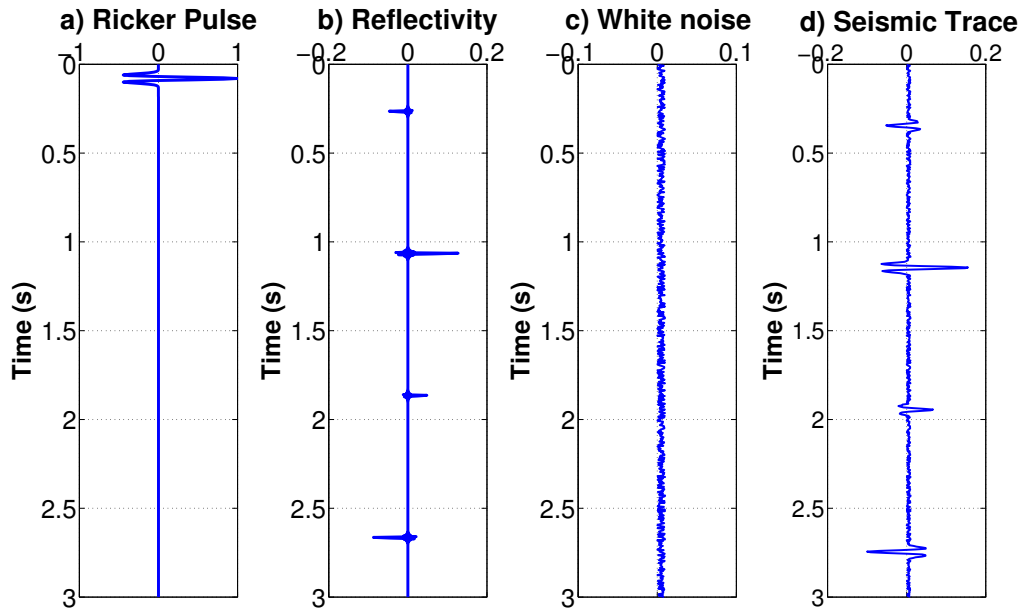
Source: From author.

3.1 Application of the deterministic extraction of the wavelet

Concerning to the deterministic wavelet extraction, the input to the *wavelet_extraction* function to extract the wavelet is the reflectivity series, the seismic trace, the length of the wavelet and a increment. The function builds a filter that when convolved with the reflectivity produces the best match between this convolution (filter and reflectivity) with the real seismic trace, given the filter length and the increment. Hence, the filter is the wavelet estimated. In our algorithm we selected a range of filter length and increment to perform the extraction of the wavelet that gives the best match between the synthetic trace and the real trace. The same procedure was performed on the real data set.

The similarity between the synthetic trace and the real trace shows that the function was very effective on estimate the wavelet for the synthetic layer model. For the modeled seismic trace with noise, the correlation coefficient between the synthetic and the real trace, was 0.981 (see Figure 7) . On the other hand, for the seismic trace without noise, the wavelet extracted was exactly the same as the Ricker pulse used to generate the real trace. The correlation coefficient was 1 (see Figure 6).

Figure 6 – Estimated deterministic wavelet for the modeled seismic trace with noise. The correlation coefficient between the synthetic trace and the real trace is 0.981.
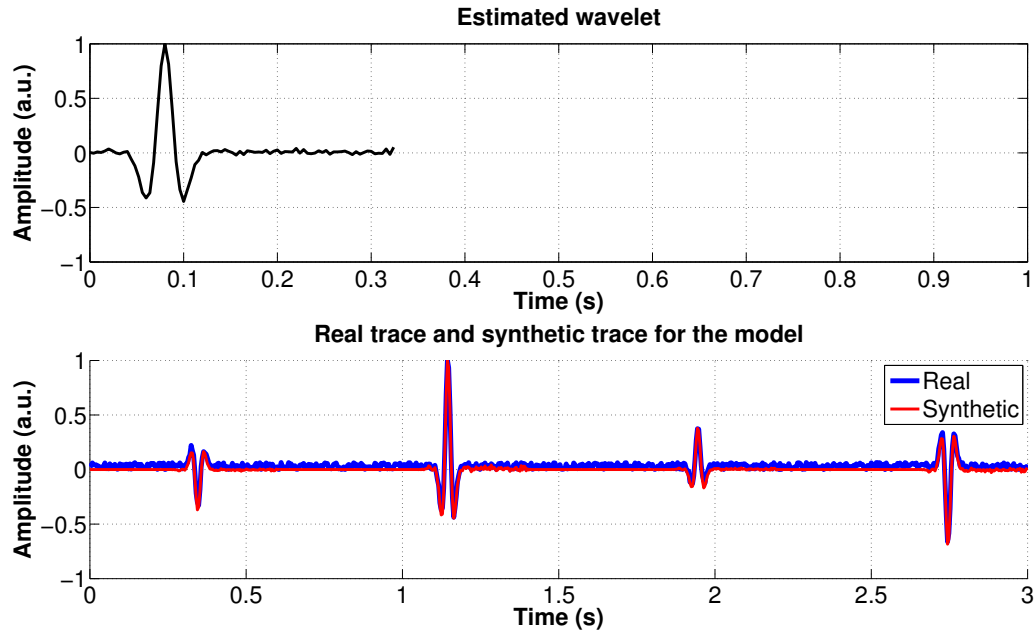
Source: From author.

Figure 7 – Estimated deterministic wavelet for the modeled seismic trace without noise. The correlation coefficient between the synthetic trace and the real trace is 1.
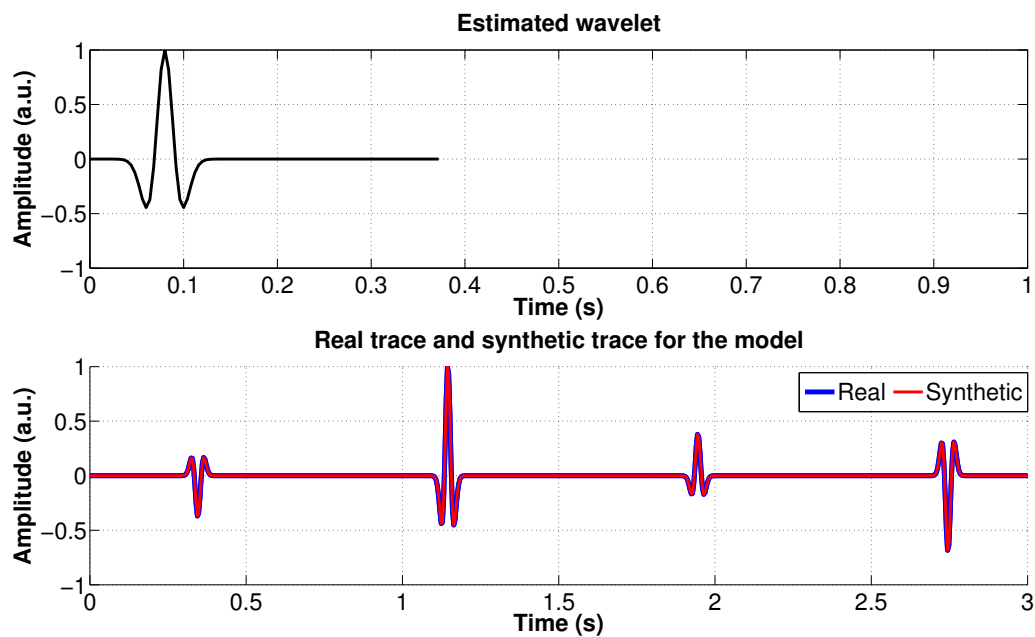
Source: From author.

3.2   Application of the least squares inverse filtering

The next test performed on the synthetic model, was related to the least squares inverse filtering to recover the reflectivity and test our algorithm of the Wiener filter. The Figures 8 and 9 shows the input trace, the desired zero lag spike output, the real output from the deconvolution and its respectively amplitude spectrums. As the distribution of energy of the desired output is not similar to that of the input trace, the real output of the deconvolution is very noisy and its amplitude spectrum is not similar to that of the input trace. However, when the desired output is changed to a spike with a arbitrary lag at 0.36 s (see Figures 10 and 11), the desired output has a distribution of energy similar to the input trace. It causes their amplitude spectrum to be also similar, therefore, the real output of the deconvolution is less noisy.

Figure 8 – The input trace, the desired output - a spike at zero lag -, and the real output of the deconvolution.
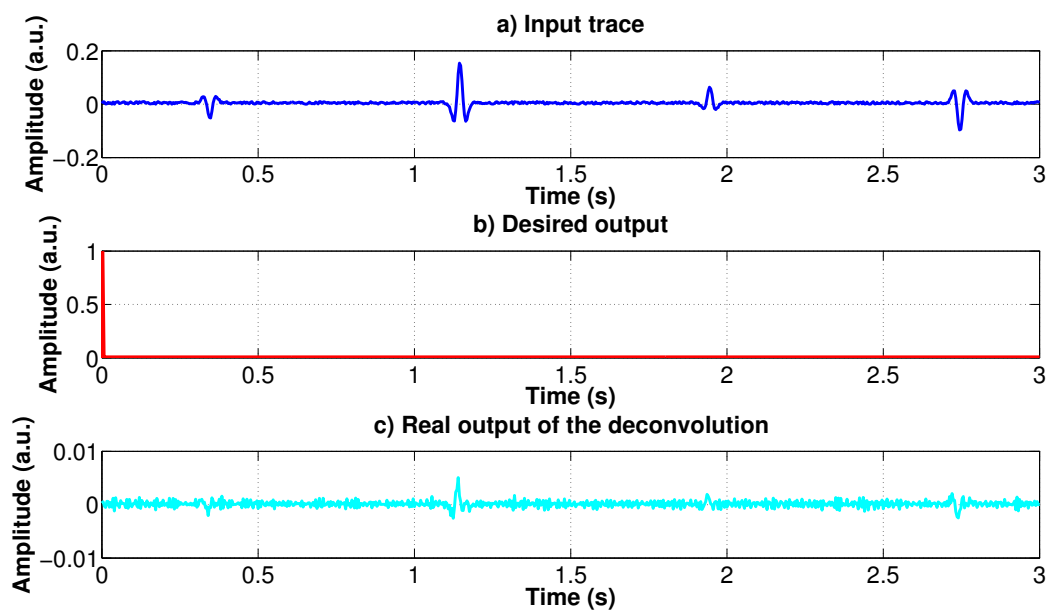
Source: From author.

3.3   Application of the predictive deconvolution

Through the normal equations of the optimum Wiener filter, the other test made on the synthetic model was the predictive deconvolution. As explained before, it aims to separate the "white" components and the minimum-delay components of the trace, which contains the wavelet. The procedure to perform the predictive deconvolution on the synthetic model was identical to that applied on the real seismic data. We selected

Figure 9 – The amplitude spectrum related to Figure 8.
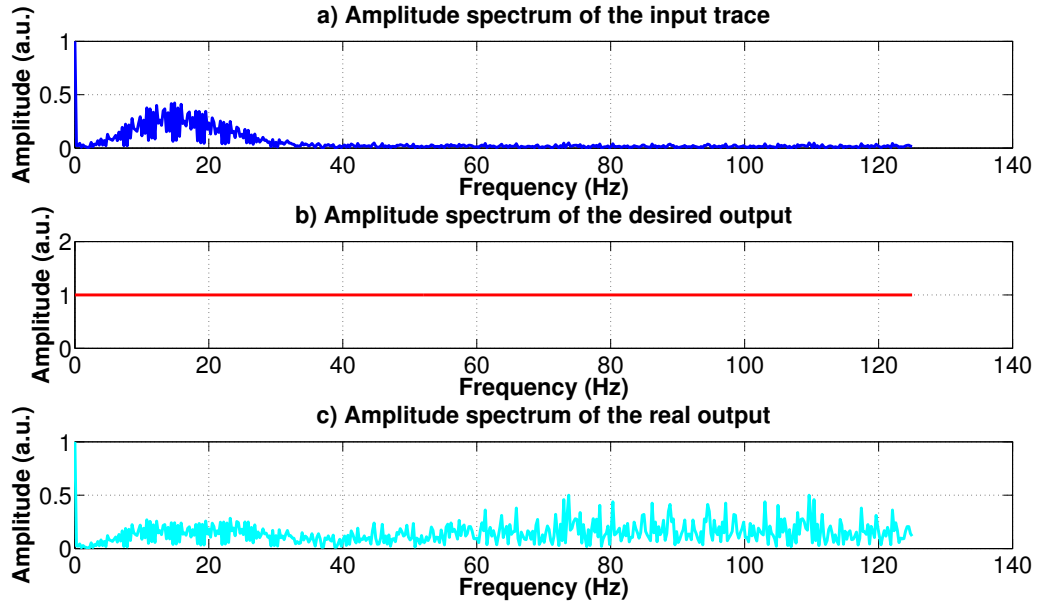
Source: From author.

Figure 10 – The input trace, the desired output - a spike at an arbitrary lag -, and the real output of the deconvolution.
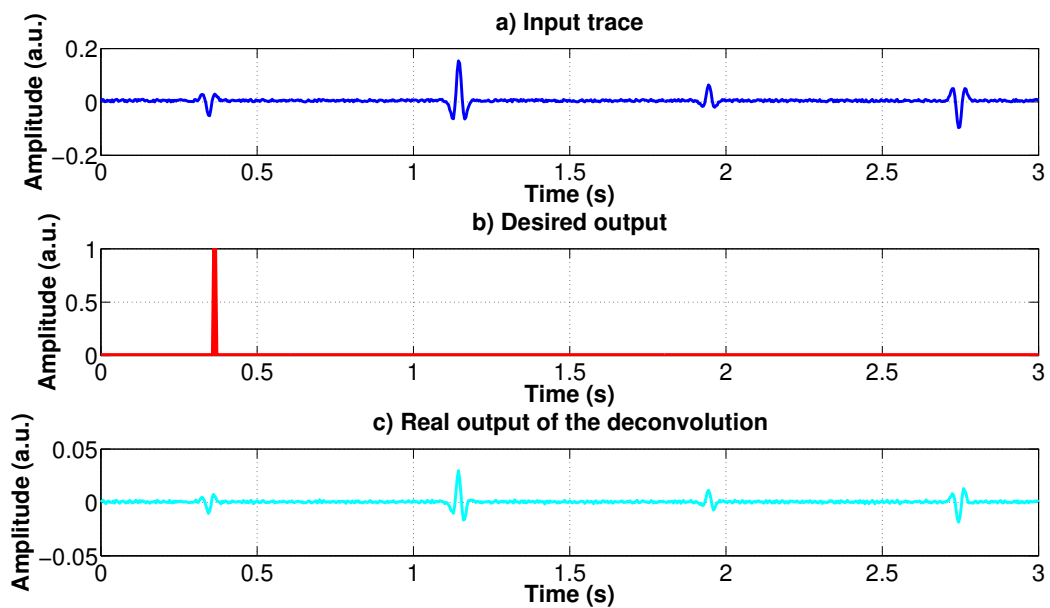
Source: From author.

Figure 11 – The amplitude spectrum related to Figure 10.
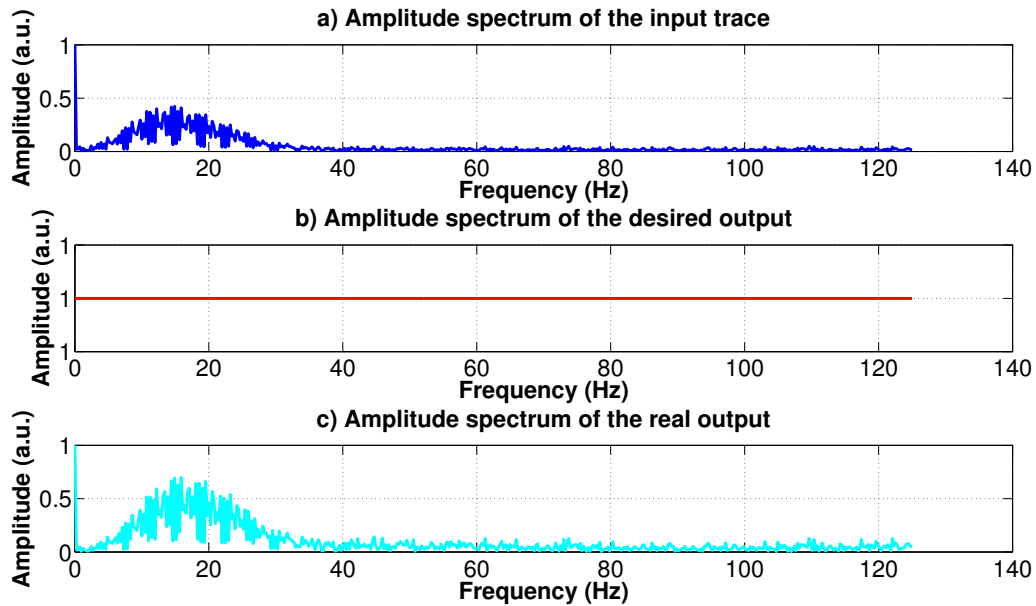
Source: From author.

a segment of the trace that we believe to be a result of a reflector. That segment is deconvolved in order to separate the white components from the wavelet, by choosing a prediction lag and the operator length.

According to Yilmaz (2000), under the ideal conditions, the resolution on the output from the predictive deconvolution can be controlled by adjusting the prediction lag α. Unit prediction lag implies highest resolution while a larger prediction lag implies less than full resolution. However, in reality, these assessments are dictated by the signal-to-noise ratio. In our algorithm we selected a range of operator length and a range of prediction lag to perform the deconvolution and then estimate the wavelet. The algorithm calculates the prediction lag and the operator length that produces the best match between the synthetic trace and the real trace. Using those parameters, we can generate the best wavelet to convolve with the reflectivity. This procedure was made on both seismic traces with and without noise.

Figure 12 shows the trace obtained by the synthetic layer model. We selected 136ms of the complete trace, from 280ms to 416ms and on that segment we perform the predictive deconvolution in a range of operator length and prediction lag. After we know the best operator length and prediction lag, we can calculate the estimated wavelet. As the amplitude spectrum (see Figure 13) of the output of the deconvolution gets similar do that of the input segment, the better the resolution of the wavelet. Figure 14 shows the comparison between the real and predicted trace. As it can be seen, they are similar even in amplitude magnitude.

Figure 12 – a) Complete seismic trace with noise from the layer model. b) The segment chosen to perform the predictive deconvolution. c) Estimated wavelet through the predictive deconvolution.
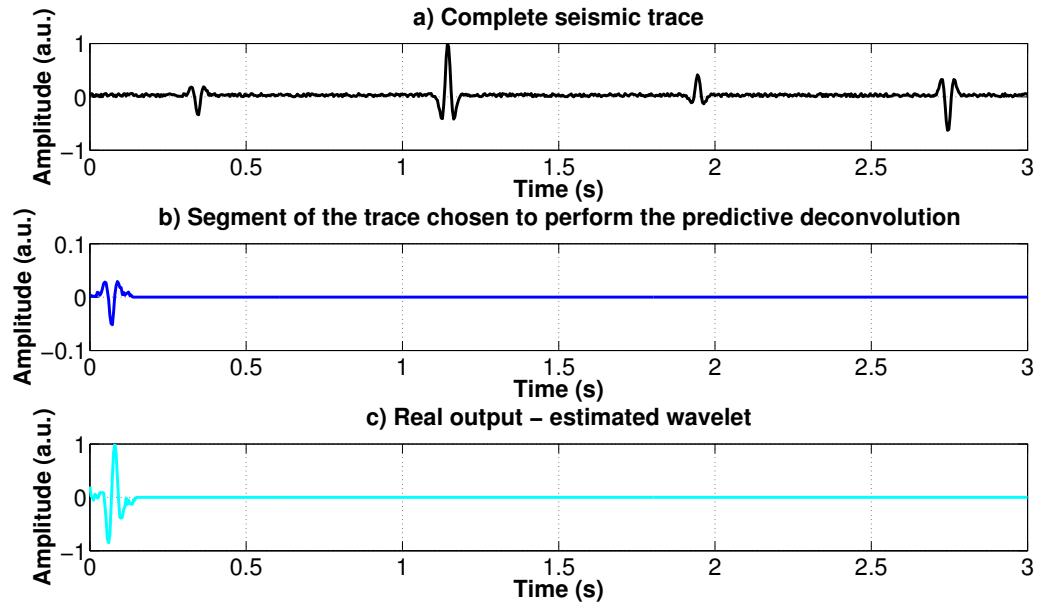
Source: From author.

Figure 13 – Amplitude spectrum related to Figure 12. The similar the spectrum of the estimated wavelet with the spectrum of the input segment and the Ricker pulse, the better the resolution of the wavelet.
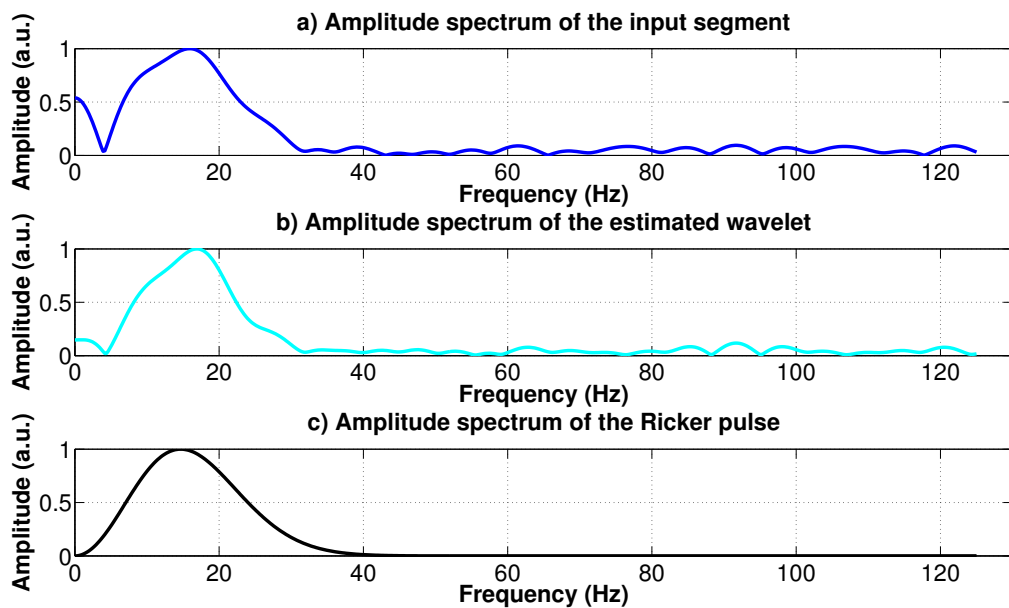
Source: From author.

Figure 14 – The estimated wavelet by the predictive deconvolution for the modeled seismic trace with noise and the comparison between the real trace and the synthetic trace. The correlation coefficient between the traces is 0.93.
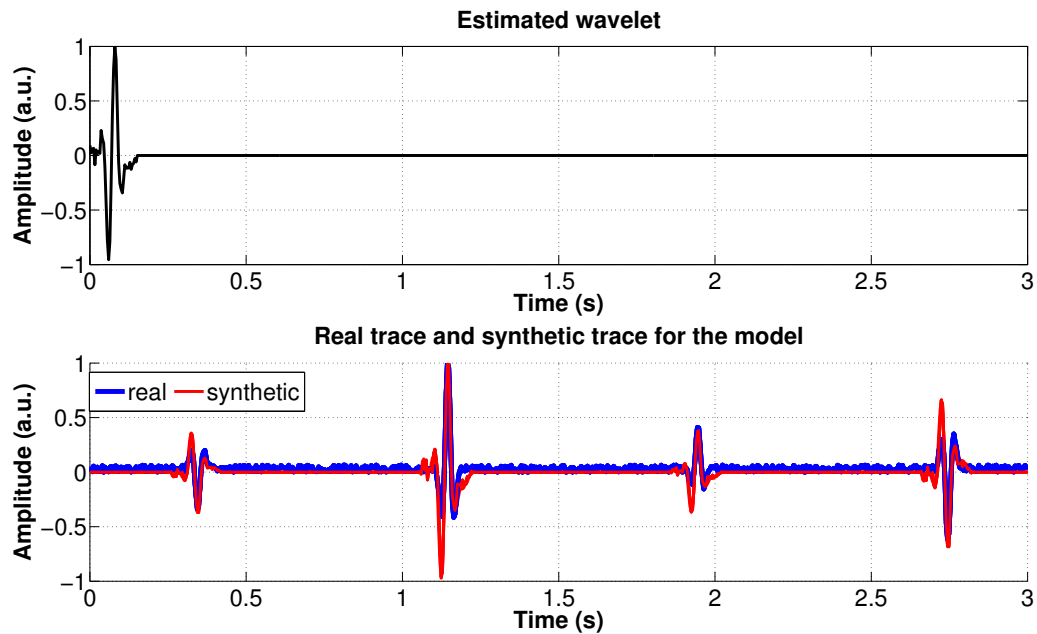
Source: From author.

This procedure was also done on the modeled seismic trace without noise (see Figures 15 and 16). The segment chosen to perform the predictive deconvolution was the same. Figure 17 shows the comparison between the real and predicted traces. As it can be seen, they are similar in amplitude magnitude.

By the results of the estimative of the wavelet on the synthetic layer model, it is possible to observe that the deterministic method produces a more accurate wavelet than the statistical method by the predictive deconvolution. It happens because the deterministic method uses both data, from the well log and from the seismic. The statistical method to estimate the wavelet is based on assumptions made about the characteristic of the wavelet (minimum-phase) and the reflectivity of the earth (random process), generating a statistical model for it purely based on mathematical tools. Therefore, this difference of accuracy of the wavelets is also expected when applying the algorithms to the real data set.

Figure 15 – a) Complete seismic trace without noise from the layer model. b) The the segment chosen to perform the predictive deconvolution. c) Estimated wavelet through the predictive deconvolution.
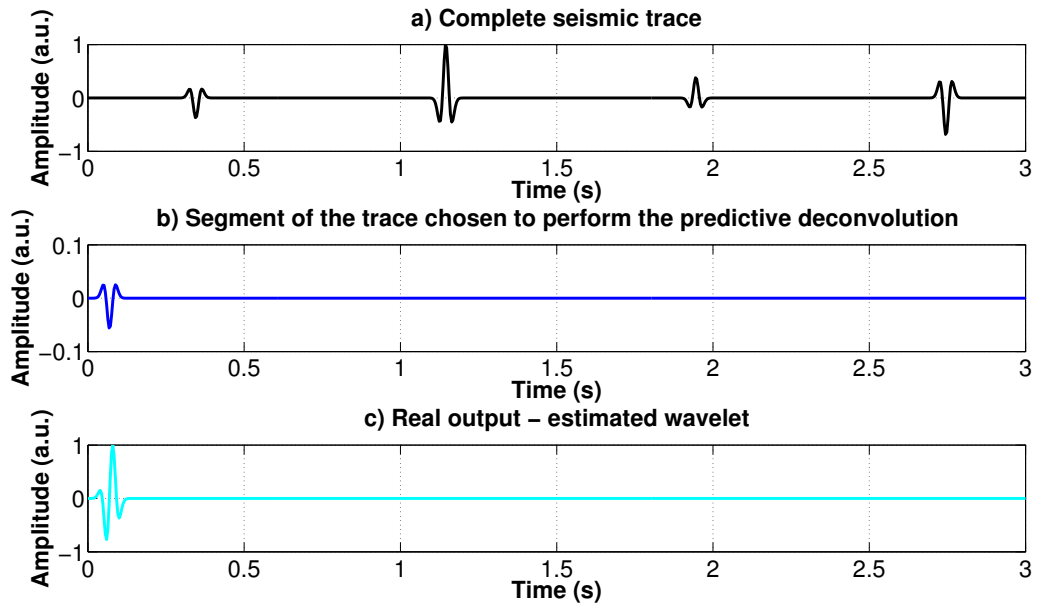
Source: From author.

Figure 16 – Amplitude spectrum related to Figure 15.
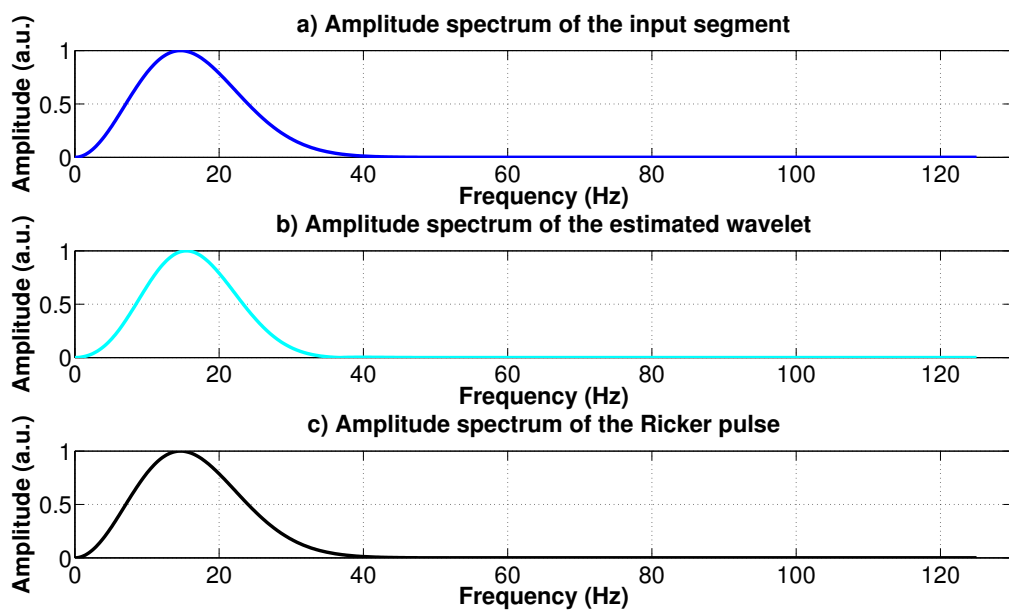
Source: From author.

Figure 17 – The estimated wavelet by the predictive deconvolution for the modeled seismic trace without noise and the comparison between the real trace and the synthetic trace. The correlation coefficient between the traces is 0.962.
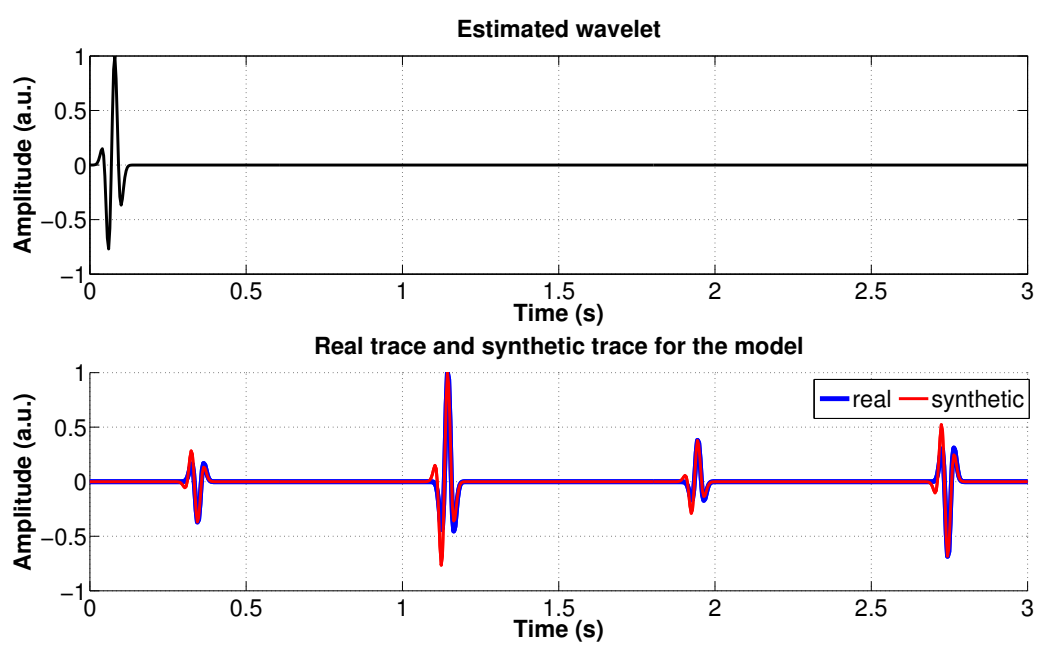
Source: From author.

4 RESULTS ON VIKING GRABEN DATA SET

4.1 Geological Backgound

The real data used in this study comes from the northern North Sea basin, Viking Graben. It is a north-south trending linear trough straddling the boundary between the Norwegian and UK sectors of the northern North Sea (MADIBA; MCMECHAN, 2003). Figure 18 shows the map where the Viking Graben field is located.

The North Viking Graben formed as a result of late Permian to Triassic rifting; extensional episodes and accompanying sedimentation continued through the Jurassic into the Early Cretaceous. The extensional episode in the beginning of Jurassic causes the Pangea to break into two continents, Gondwana and Laurasia. During this period the sea level rose. The burial of algae and bacteria below the mud of the seafloor resulted in the formation of the oil and gas of the North Sea. The Jurassic transgressive system has periods of regression that provided the coarse clastic input that forms the reservoir intervals separated by deepwater shales (MADIBA; MCMECHAN, 2003). The depositional environments of the Jurassic reservoirs range from fluvial to deltaic and shallow marine. The Jurassic was a period of active faulting; hydrocarbon traps are usually fault-bounded structures, but some are associated with stratigraphic truncation at the unconformity at the base of the Cretaceous (KEYS, 1998). This unconformity - referred as BCU - is located above the Jurassic synrift sediments that are also overlain by Cretaceus and Tertiary basin fill. The Paleocene reservoir in the North Viking Graben is characterized by deepwater clastics. The Paleocene interval is undisturbed by the rift tectonism and dips gently into the basin (KEYS, 1998). The sediments were deposited in a slope environment and so contains turbidites (MADIBA; MCMECHAN, 2003).

4.2 Seismic and well logs data

The study area is in the North Viking Graben in the North Sea Basin. The seismic line consists of 1001 shot records, each shot recorded on 120 channels for six seconds. The sample rate is of 4ms. An air gun provided the seismic source. The source and receivers are separated by 25m. The seismic data has 2142 CMPs with 1501 samples each. The well log information is from two wells designed Well A and Well B located in the seismic line. The well A is located on CMP 808 and well B on CMP 1572. According to Madiba e McMechan (2003), the major base Cretaceous unconformity (BCU) is located at approximately 1.9s in well A and at 2.4s in well B. Figure 19 shows the interpreted seismic section migrated in time by Monroe e Figueiredo (2015).

Figure 18 – Map from the Viking Graben area.
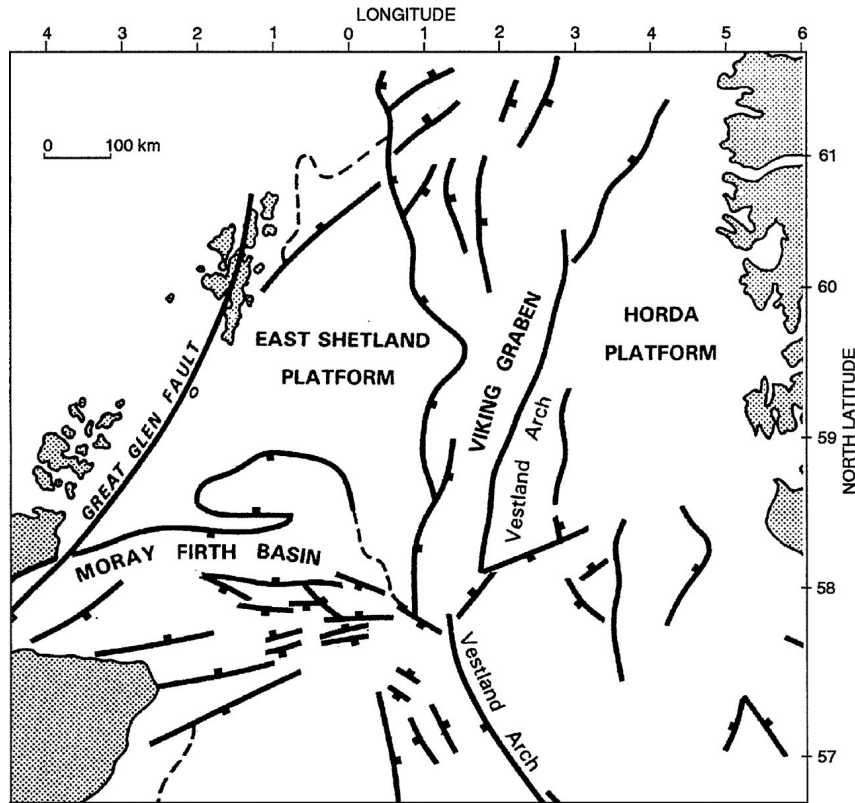
Source: from Madiba e McMechan (2003).

Due the unregistered points or noises in the density and sonic data, it was necessary to edit these logs in order to do not deal with wrong values. Because of that, a despike process was applied on both well logs (see Figures 20 a and b). The procedure to perform the despike is to set a limit value for the spikes on the sonic and density log. If the measured point does not exceeds that limit, the value of the real log is used. If the measured point exceeds that limit, the value of the smoothed log is used.

As on well B the information about density log was insufficient, it was completed using the Gardner's relation (GARDNER, 1974) that relates compressional velocity with the bulk density of the lithology where the wave travels. It is given by,

$$\rho = 0.31 V_p^{0.25}, \tag{4.1}$$

where V_p is in m/s and ρ in g/cm^3.

Three-component zero-offset vertical seismic profile were recorded in wells A and B (KEYS, 1998). In this case, the Vertical Seismic Profiles (VSPs) are useful in the well tie process once they provide a link between wells and seismic at the correct scale. A string of geophones is deployed in the well and by shifting them up between shots, it is possible to record signals at several levels. At each level, the geophones will record waves, including the direct arrival. With the measurement of the arrival time for the direct wave arrival, at each level in depth, it is possible to establish a time-depth relationship. The time-depth

Figure 19 – Time migrated and interpreted seismic section of the Viking Graben field. As can be seen, the main geological structures, faults, anomalies and geological facies are depicted.
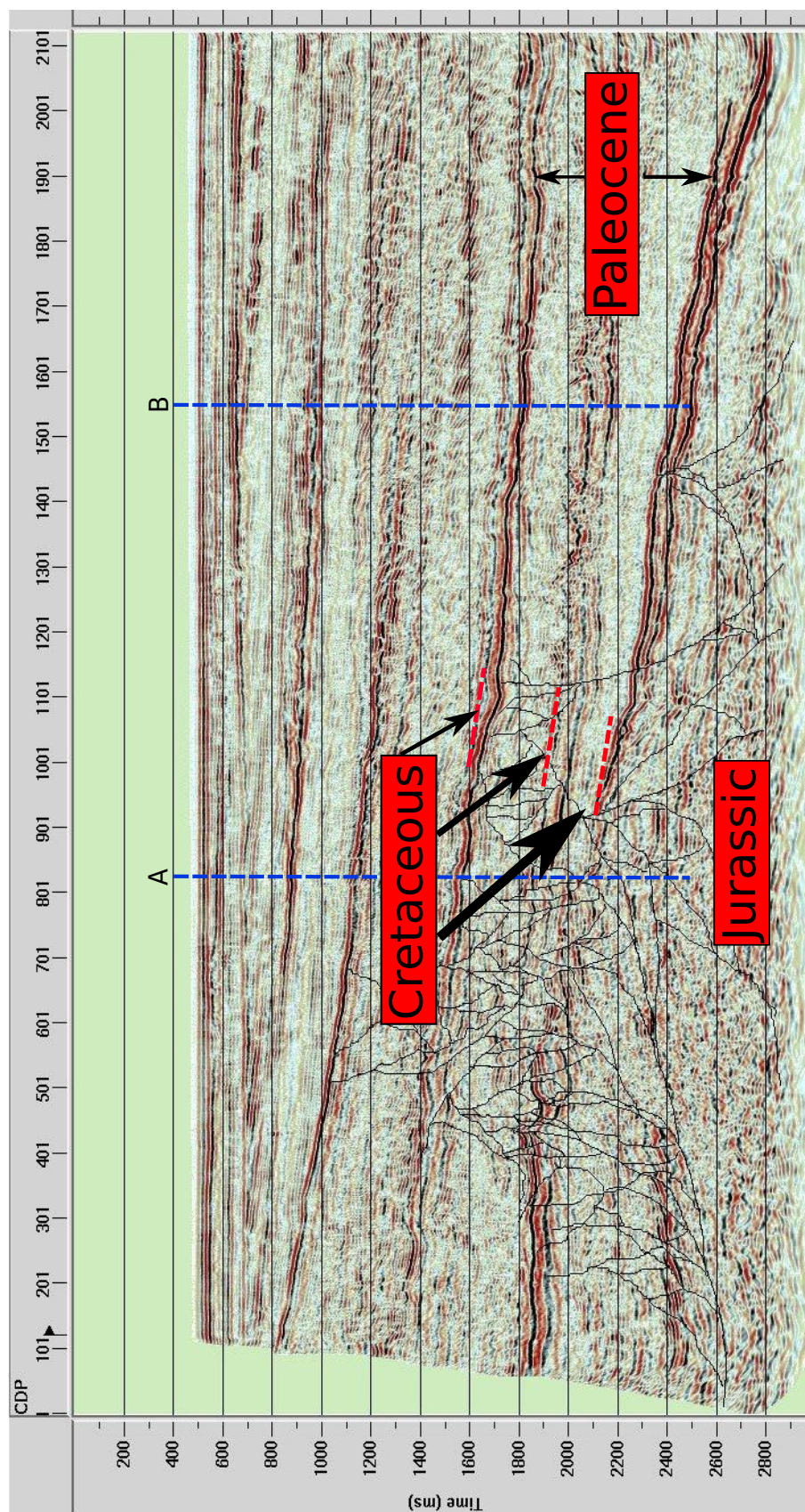
Source: From Monroe e Figueiredo (2015).

relationship in this study was generated by time picks of the VSP direct arrivals. The data set for both, Well A and Well B contained pairs of time-depth that was used to select a segment of depth on the wells logs that corresponds to a selected segment of time on the seismic trace. Figure 21 shows the time-depth relationship for wells A and B.

Figure 20 – The logs used to construct the synthetic seismogram at (a) well A and (b) well B. From left to right: sonic log (P-wave velocity), density log and reflectivity log. The red lines are the output logs from the despiking process.

(a)

(b)
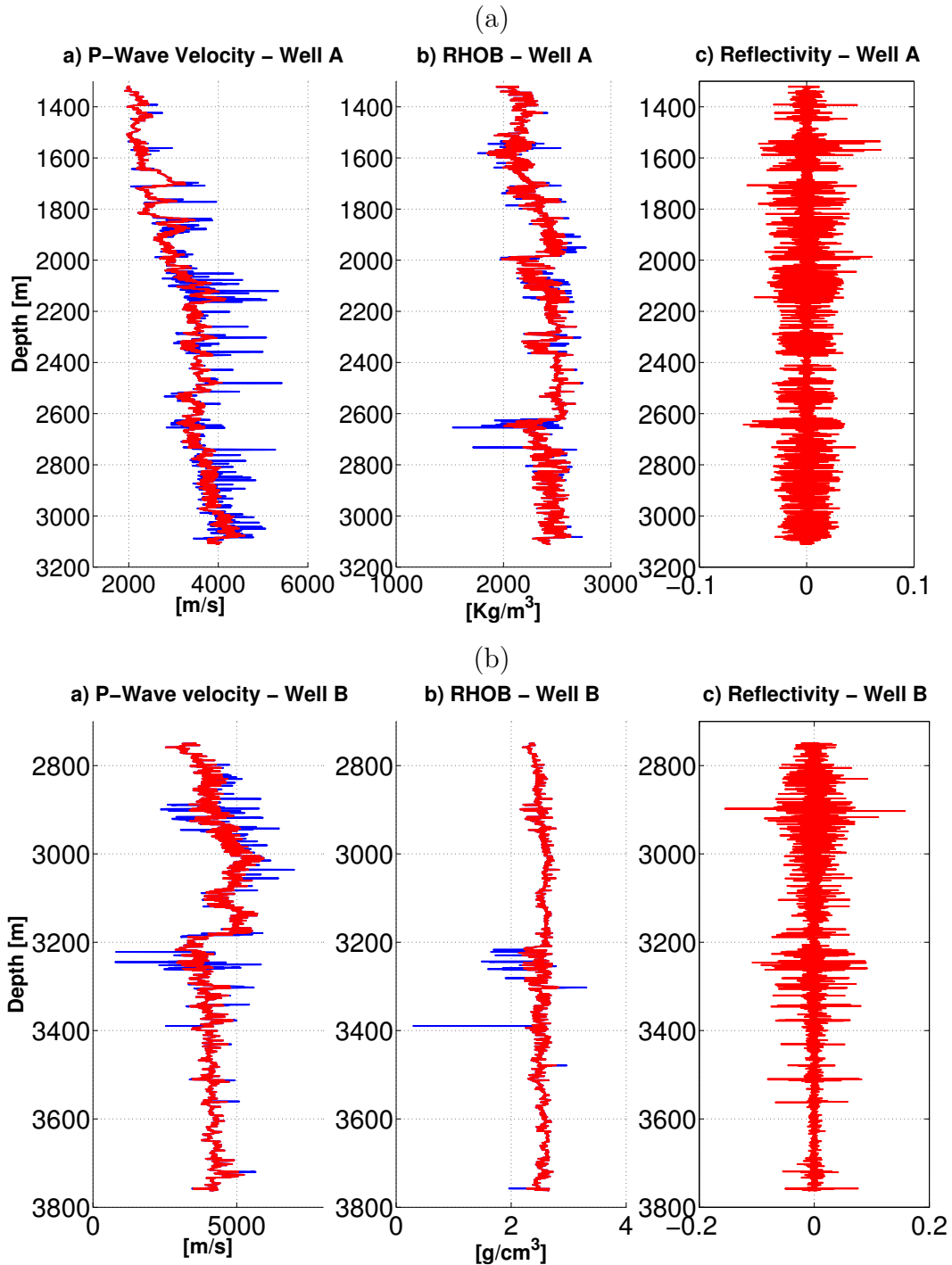
Source: From author.

Figure 21 – Time picks of the VSP direct arrivals that constitute the time-depth relationship for wells A and B.
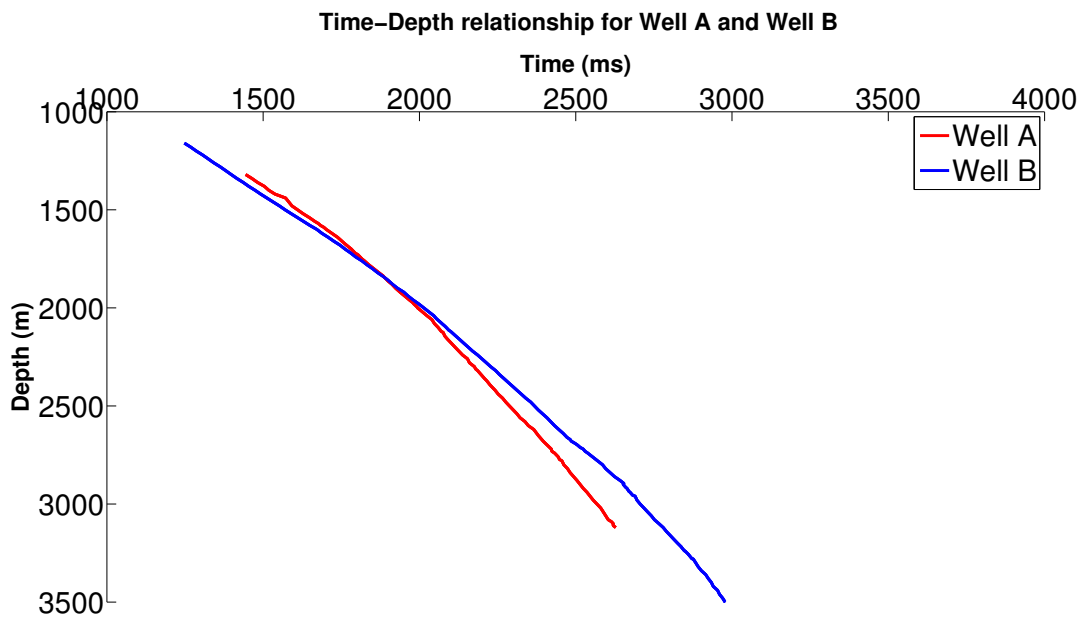
Source: From author.

It is possible to measure the quality of the tie through the correlation coefficient. According to White (2003), the best match location (higher correlation coefficient of the synthetic seismogram with the real seismic trace from a CMP) often does not occur at the well location. If the seismic data was time migrated, since velocity typically increases with depth, time migration commonly moves the best match location up-dip from the well. The best match location is found by scanning a number of traces around the well for the correlation coefficient (SIMM, 2014). On the well to seismic tie from the work of White (2003) the best match location of the well tie is about 100m distant from the well, with a correlation coefficient between the seismic trace and the synthetic trace was 0.790. For this same data, Ma Roy E. White (2010) performed a wavelet estimation based on the best matching well-log, VSP and surface-seismic data over different time intervals at the best match location, that on their work, was about 50m NE of the well.

White, Simm e Xu (1998) perform a well to seismic tie, AVO modeling and fluid substitution on a area from the North Sea oilfield. On their work, the best match location for the well to seismic tie was on CMPs 732 and 734, very close to the posted well location that is on CMP 735. The well to seismic tie was performed on both well logs A and B with a stack seismic section and with a time migrated seismic section. The first analysis was regarding the well A and the result of the well tie for both seismic sections with the both methods to estimate the wavelet. The reflectivity series used to create the synthetic seismogram was the same for both deterministic and statistical method to estimate the wavelet. The same procedure was applied to the well B.

The estimative of the wavelet for the well A through the predictive deconvolution followed the same methodology applied to the synthetic model. We selected a segment of the seismic trace and deconvolved that segment to estimate the wavelet. The input parameters of our algorithm is the prediction lag, the length of the deconvolution operator and the seismic traces in the vicinity of the posted location of the well, which for the Well A is the CMP 808. We chose a range of prediction lag and a range of operator length to perform the predictive deconvolution on the segment of the seismic trace. The algorithm returns the best pair prediction lag and operator length that produces the wavelet responsible for the highest correlation coefficient between the seismic trace and the synthetic trace. The prediction lag can be adjust to improve the resolution of the output of the deconvolution and the operator length can improve the output as it gets longer, however, longer operator length can also introduce noise on the output. Moreover, the operator length have a limit beyond which it does not change the resolution of the output, and therefore, the correlation coefficient between the seismic and the synthetic traces. In fact, the relations of the prediction lag and the operator length are dictated by the signal-noise ratio.

4.3 Stacked seismic section - Well A

As mentioned before, the first analysis consists to compare the results of the statistical and deterministical wavelet estimation and the respective well to seismic tie on a stack section concerning the location and information of the well A. The procedure to estimate the wavelet through the predictive deconvolution was the same as the one applied on the synthetic model: a segment of the seismic trace is selected and on that segment the predictive deconvolution is performed with the proposal to separate the signal related to the seismic source and the signal related to the reflectivity of the earth. The algorithm gives the best pair prediction lag (α) and operator length (N) that produces the best wavelet for the synthetic trace. To measure the quality of synthetic trace, we correlate it with the real trace. We followed the recommendation of White (2003), and we selected traces on the vicinity of the posted well location (CMP 808) to find the best match, once it is common for the best match to do not be located on the well location.

Figure 22a shows that the best well to seismic tie location with the highest correlation relying on CMP 809 instead CMP 808, as mentioned in Keys (1998). Figure 22b shows the prediction lag versus correlation coefficient. As can be noted the highest correlation corresponds to the prediction lag of 38 ms. Finally, the Figure 22c shows the operator length versus correlation coefficient. In this case the highest correlation yielded was with a operator length of N=118 ms.

Figure 23a shows the estimated wavelet based on the statistical method. A convolution with reflection coefficient (shown in Figure 20 was performed in order to reach the synthetic seismic trace. Figure 23b shows the synthetic seismogram (red) aligned to the seismic trace (blue).

In order to have a frequency content on the synthetic trace similar to that on the real seismic trace, the second approach concerning to the predictive deconvolution was to compute a average wavelet. It was selected four different segments along the seismic trace to perform the predictive deconvolution and consequently four wavelets were estimated. These wavelets as well as the average wavelet is shown in Figure 24. The wavelet used to compute the synthetic trace was an average among all the four estimated wavelets. Figure 25 illustrates the average wavelet and the convolution of it with the reflectivity of Figure 20.

The other method to estimate the wavelet was deterministic. It uses both the seismic data and the well logs to estimate the wavelet that leads to the best match of the synthetic to the real seismic trace. As shown at Figure 26 the best match relies on CMP 809. Figure 27 shows the deterministic estimative of the wavelet as well the comparison between the real and estimated trace. As can be seen, the improvement of the well to seismic tie, is verified by increasing in correlation coefficient to 0.727.

Figure 22 – (a) Correlation coefficient x CMPs for the well A with a stacked seismic section. The best match location is on CMP 809, with a correlation coefficient of 0.635. (b) Prediction lag x correlation coefficient for the CMP 809 on a stacked seismic section. (c) Operator length x correlation coefficient for the CMP 809 on a stacked seismic section.
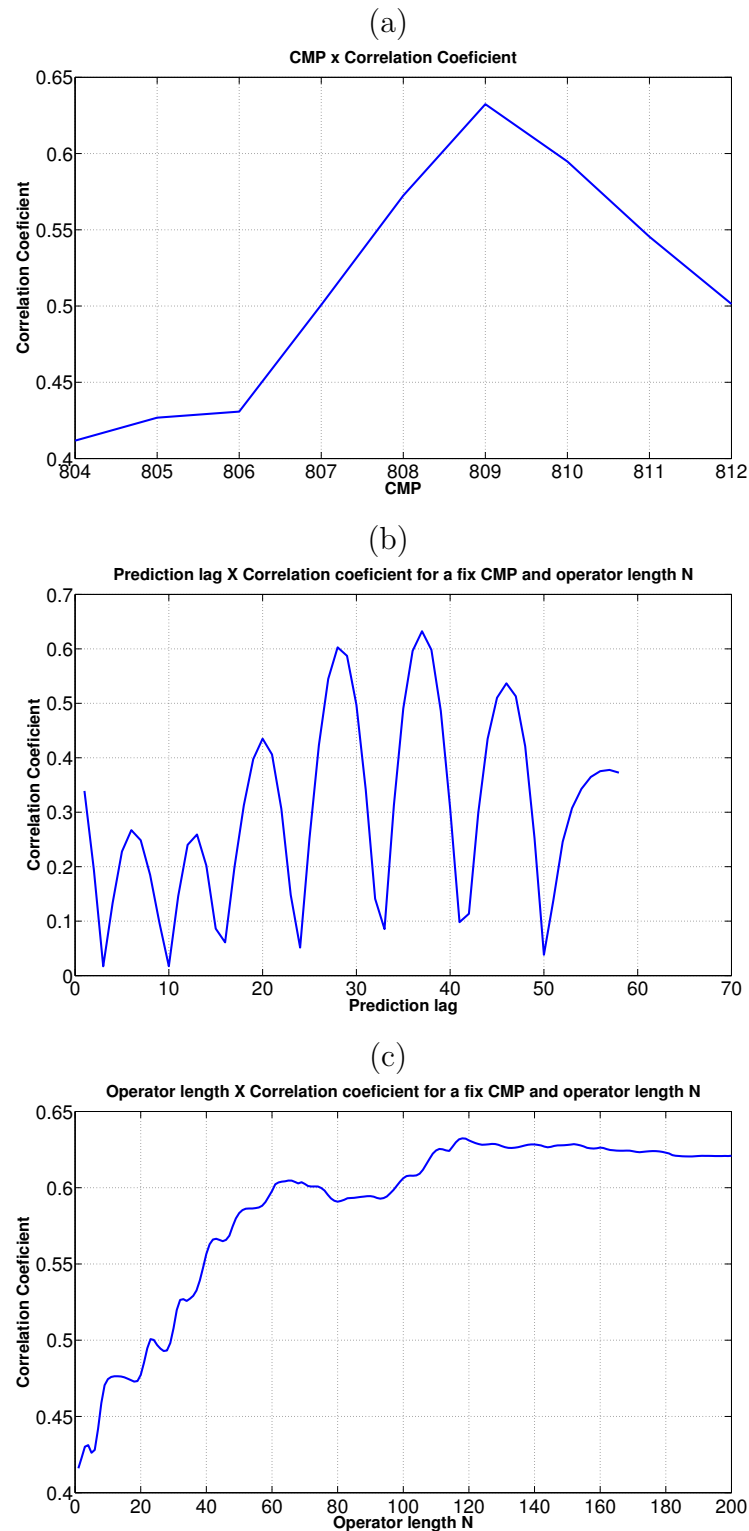
Source: From author.

Figure 23 – (a) The wavelet estimated through the statistical method and the synthetic and real stacked seismic trace on CMP 809. (b) The synthetic seismogram (red) aligned to the seismic trace (blue). The correlation coefficient was 0.635.
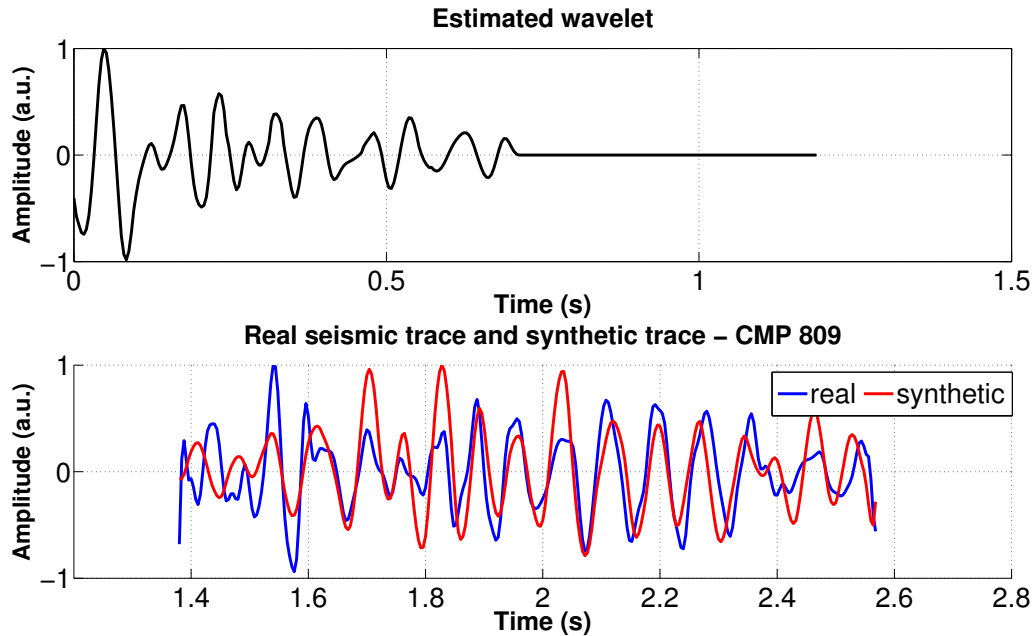
Source: From author.

Figure 24 – The wavelets estimated through the predictive deconvolution from each segment of the seismic trace and the average wavelet used to compute the synthetic trace.
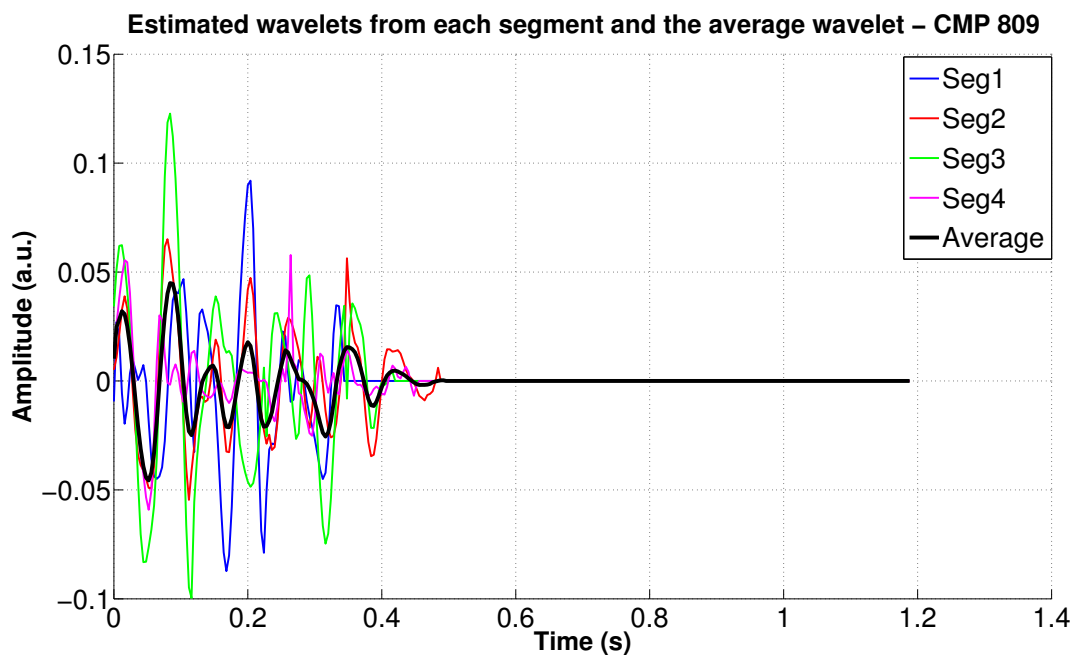
Source: From author.

Figure 25 – (a) The average wavelet estimated and the synthetic and real stacked seismic traces for the CMP 809. (b) The synthetic seismogram (red) aligned to the seismic trace (blue). The correlation coefficient in this case was 0.653.
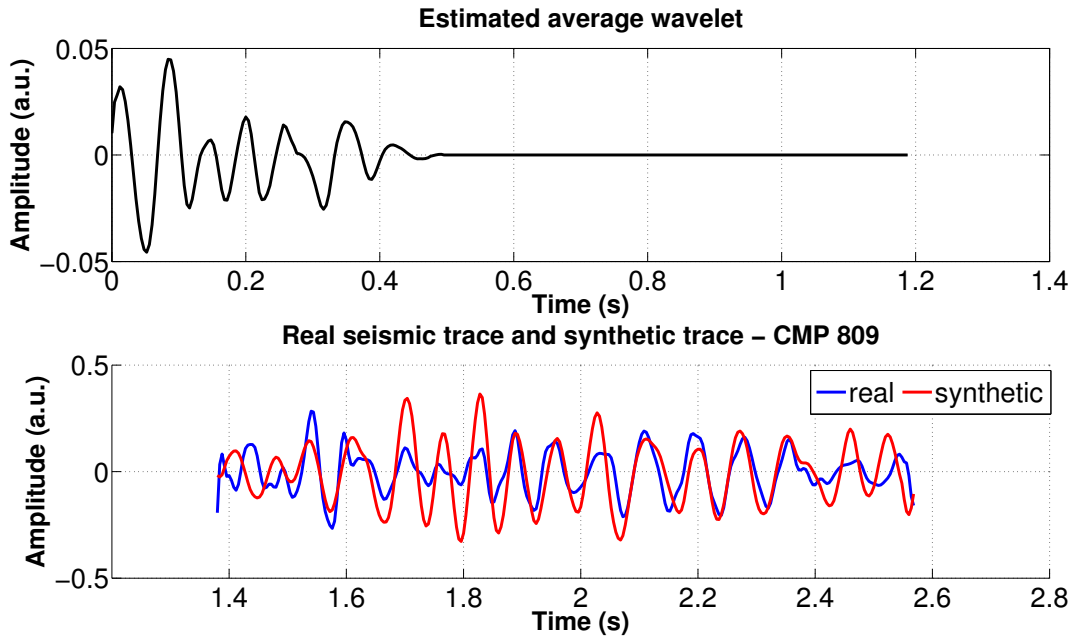
Source: From author.

Figure 26 – Correlation coefficient x CMPs for the well A with stacked seismic section using the deterministic estimative of the wavelet. The best match location is also on CMP 809, but the correlation coefficient using the deterministic approach is higher than that of the statistical approach. It was 0.727.
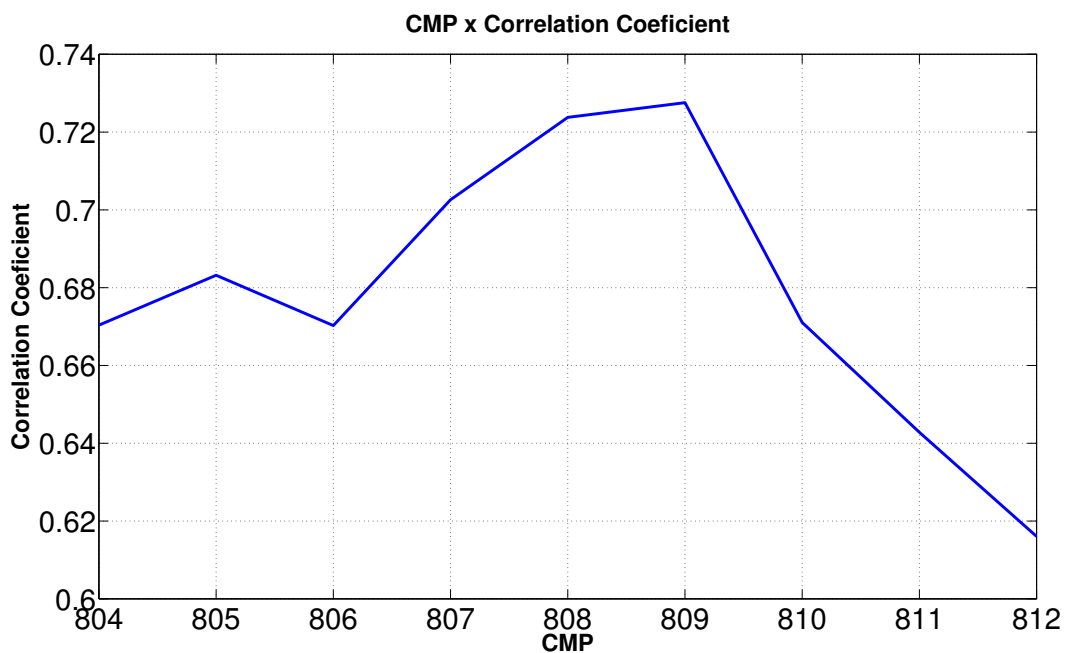
Source: From author.

Figure 27 – The wavelet estimated through the deterministic method and the synthetic and real staked seismic trace on CMP 809. The correlation coefficient was 0.727.
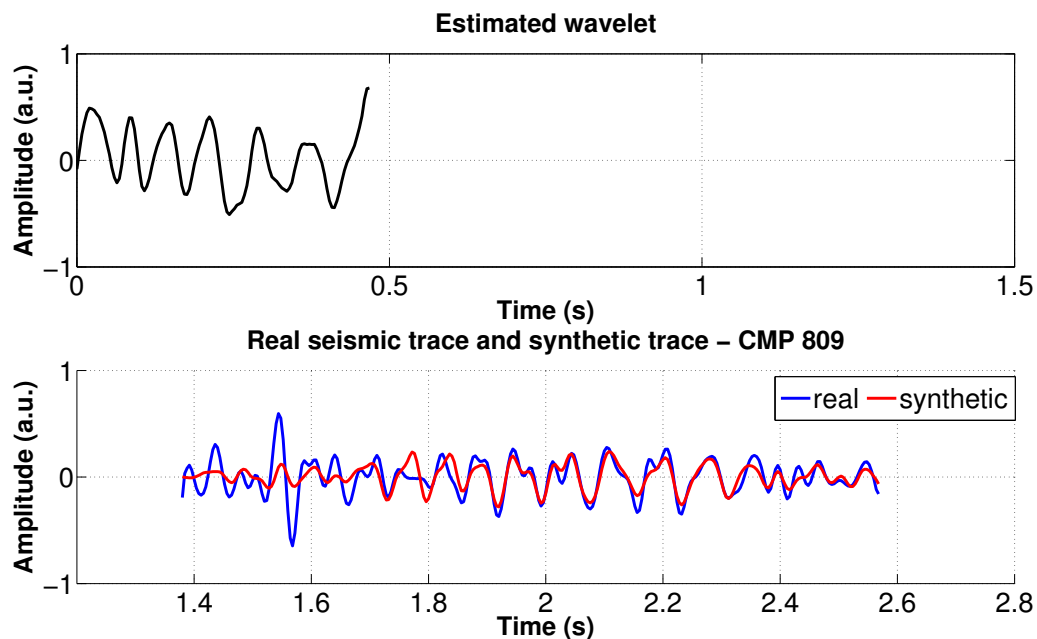
Source: From author.

4.4 Stacked seismic section - Well B

This section shows the results of the statistical and deterministic estimation of the wavelet and the respective well to seismic tie on a stacked section concerning the location and information of the well B. The corresponding location for this well is the CMP 1572. Figures 28 and 29 shows the results obtained with the predictive deconvolution method to estimate the seismic wavelet with a stacked seismic section on well B. Although the posted well location is on CMP 1572, the best match location for this well was on CMP 1573, with a correlation coefficient of 0.720. The prediction lag that yields this result was $\alpha = 51$ ms and the operator length was $N = 69$ ms.

On this well the estimation of the average statistical wavelet was also performed, such as the procedure done on well A. The results are shown on Figures 30 and 31. The use of the average statistical wavelet in this well improved the quality of the tie, once the correlation coefficient increased from 0.720 (predictive deconvolution on one segment alone) to 0.756.

Finally, the last procedure made on the stacked seismic section with the well B, was the well to seismic tie with a wavelet estimated through the deterministic method. While the predictive approach leads to the best match location on CMP 1573, the deterministic method lead to the best match location on CMP 1574, with a correlation coefficient of 0.791, as shown at Figures 32 and 33. Figure 34 shows the well to seismic tie made with a

Figure 28 – (a) Correlation Coefficient x CMPs for the Well B with a stacked seismic section using the predictive deconvolution to estimate the wavelet. The best match location for this method is on CMP 1573, with a correlation coefficient of 0.720. (b) Prediction lag x Correlation Coefficient for the CMP 1573 on a stacked seismic section. (c) Operator length x Correlation Coefficient for the CMP 1573 on a stacked seismic section.

(a)

(b)

(c)
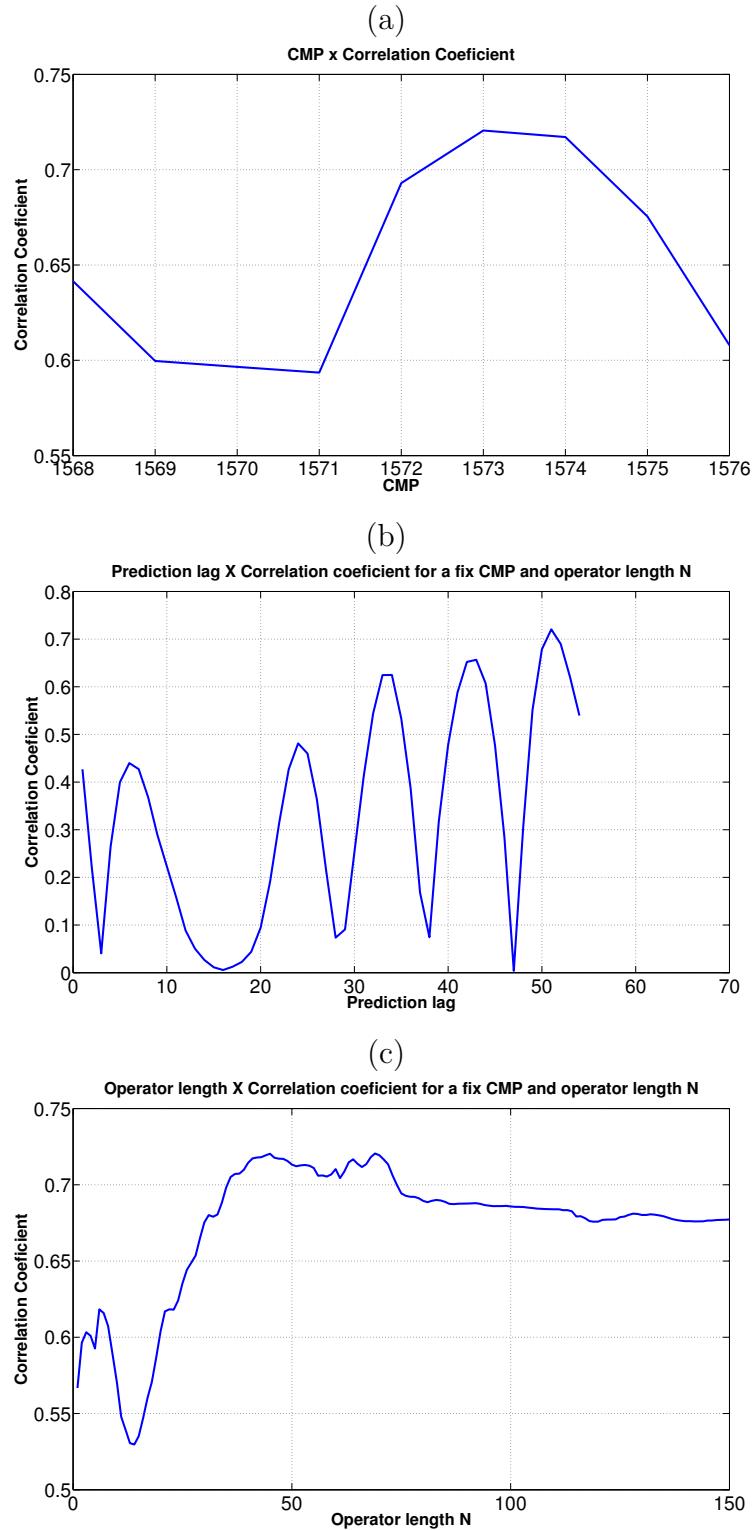
Source: From author.

Figure 29 – The wavelet estimated through the predictive deconvolution method and the synthetic and real stacked seismic trace on CMP 1573. The correlation coefficient was 0.720.
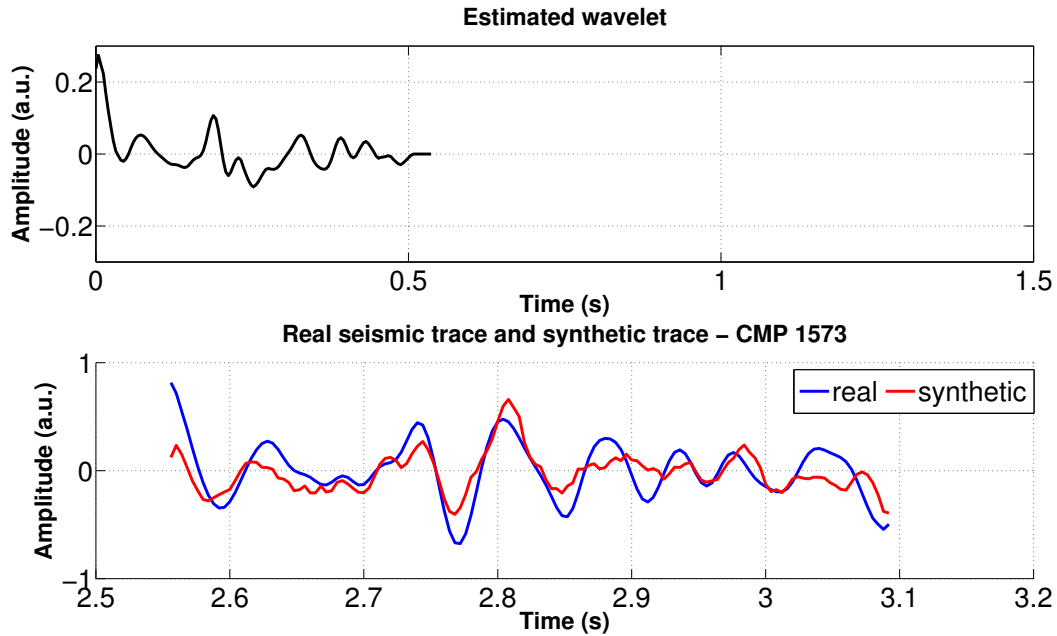
Source: From author.

Figure 30 – The estimated wavelets through the predictive deconvolution from each segment of the seismic trace and the average wavelet used to compute the synthetic trace.
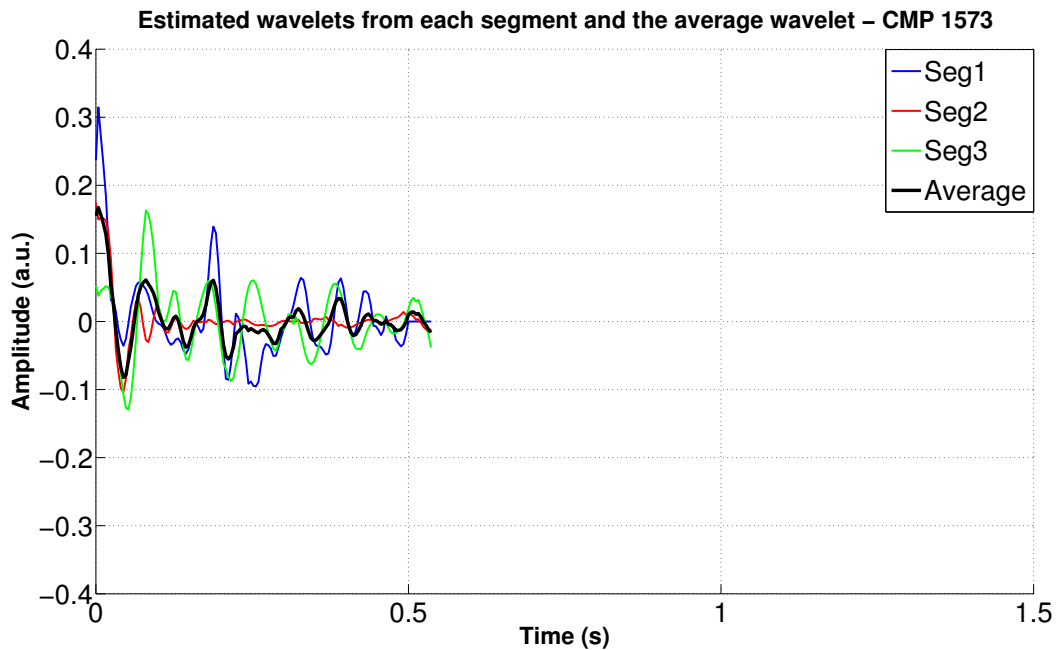
Source: From author.

Figure 31 – The average wavelet estimated and the synthetic and real stacked seismic traces for the CMP 1573. The correlation coefficient was 0.756.
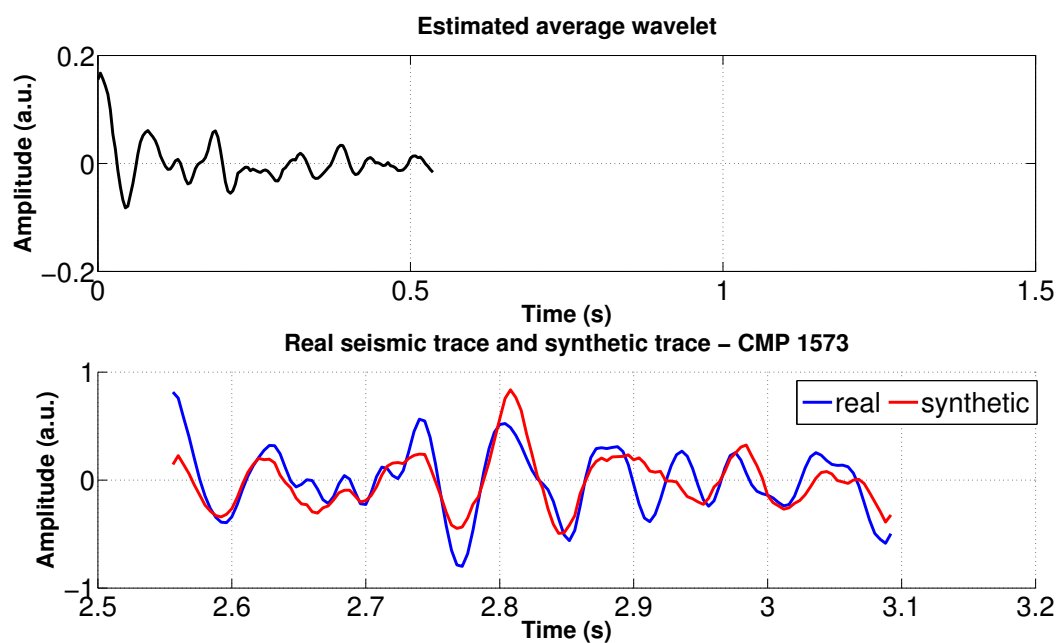
Source: From author.

deterministic estimated wavelet on the CMP 1573 wich is the best match location from the other methods.

Figure 32 – Correlation Coefficient x CMPs for the Well B with a stacked seismic section using the deterministic estimative of the wavelet. The best match location is on CMP 1574, with a correlation coefficient of 0.791. The correlation coefficient on CMP 1573, the best match location for the predictive deconvolution, was 0.758, as shown on Figure 34.
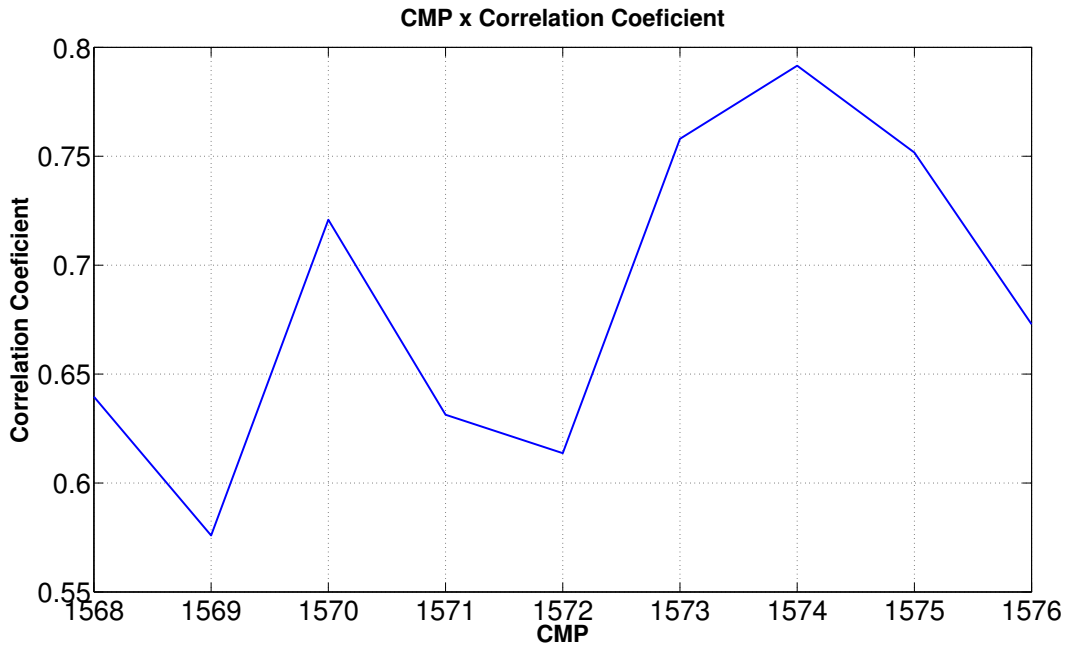
Source: From author.

Figure 33 – The wavelet estimated through the deterministic method and the synthetic and real stacked seismic trace on CMP 1574. The correlation coefficient was 0.791.
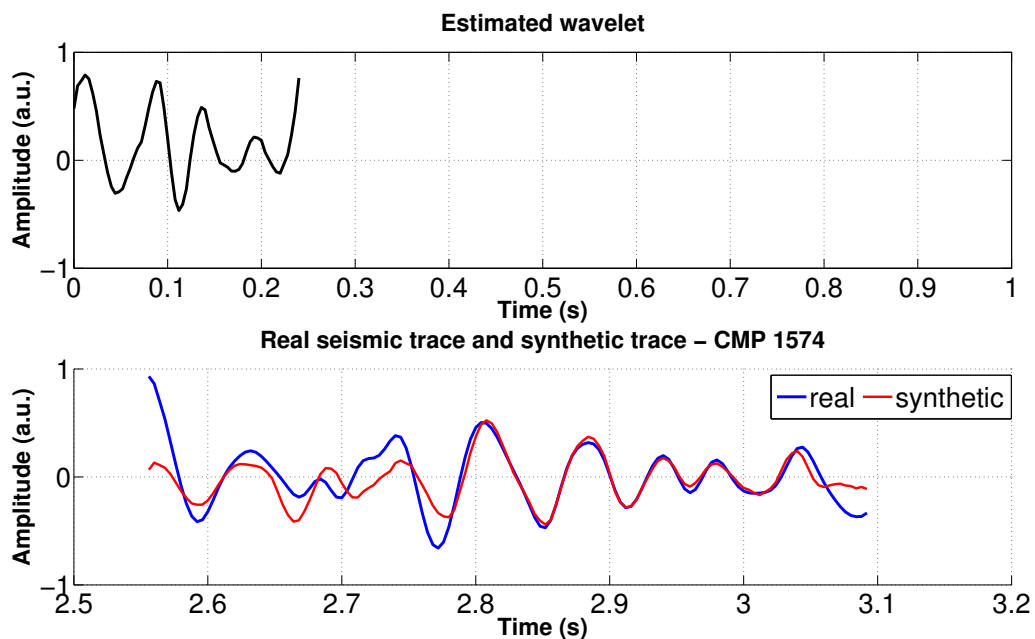
Source: From author.

Figure 34 – The wavelet estimated through the deterministic method and the synthetic and real seismic trace on CMP 1573, the best match location for the predictive estimation. The correlation coefficient was 0.758.
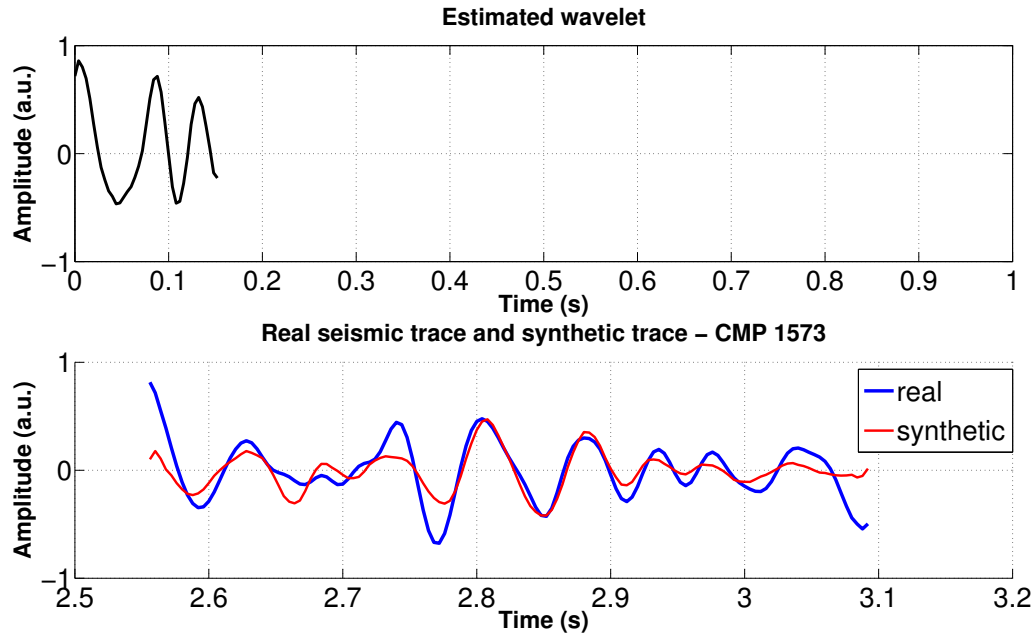
Source: From author.

4.5   Time migrated seismic section - Well A

In general, a stacked seismic section has noise due to diffractions and dip reflectors that are not positioned correctly. The migration aims to correct this effects. Hence, it is expected that the well to seismic tie on a migrated section produce better results. Obviously, the quality of the migration will affect the results of the well tie. For that reason, we test the estimative of the wavelet from both methods also on a migrated section. The results of the estimative of the wavelet through the predictive deconvolution with a migrated seismic section and information from the well A are shown on Figures 35 and 36. The correlation coefficient for this case was 0.658, higher than when using the stacked seismic section (see Figure 23). The best pair, prediction lag and operator length for this case were $\alpha = 13$ ms and N = 14 ms.

Using the migrated seismic section we also estimated the average wavelet from the predictive deconvolution from different segments of the seismic trace (see Figure 37). This method proved to yield better results on the quality to the tie also on the migrated seismic section. The correlation coefficient increased from 0.658 (using the predictive deconvolution of one segment alone - see Figure 36) to 0.674 when using the average statistical wavelet as shown at Figure 38.

The results of the well to seismic tie using the deterministic method to estimate

Figure 35 – (a) Correlation Coefficient x CMPs for the Well A with a migrated seismic section and the predictive deconvolution to estimate the seismic wavelet. The best match location is the same as for the stack seismic section, on CMP 809, but the correlation coefficient is higher, it is 0.658. (b) Prediction lag x Correlation Coefficient for the CMP 809 with a migrated seismic section. (c) Operator length x Correlation Coefficient for the CMP 809 with a migrated seismic section.

(a)

(b)

(c)
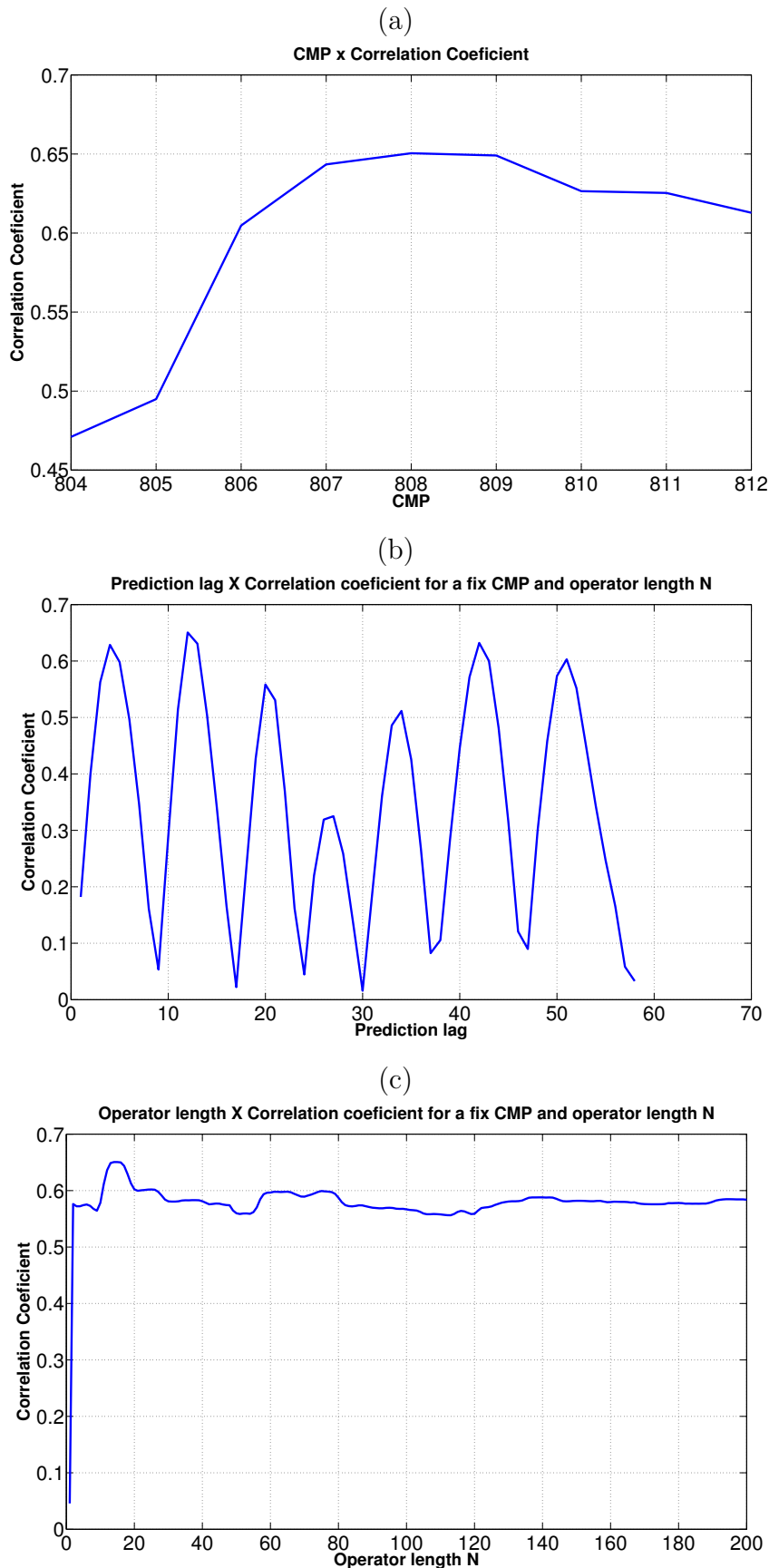
Figure 36 – The wavelet estimated through the statistical predictive deconvolution method and the synthetic and real migrated seismic trace on CMP 809. The correlation coefficient was 0.658.
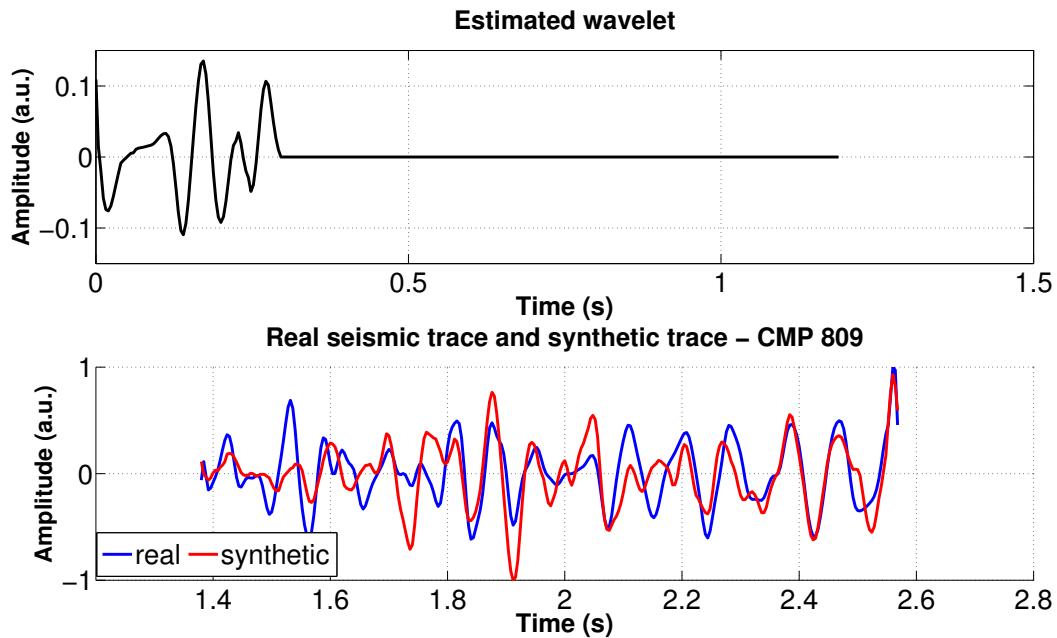
Source: From author.

Figure 37 – The wavelets estimated through the predictive deconvolution from each segment of the migrated seismic trace and the average wavelet used to compute the synthetic trace.
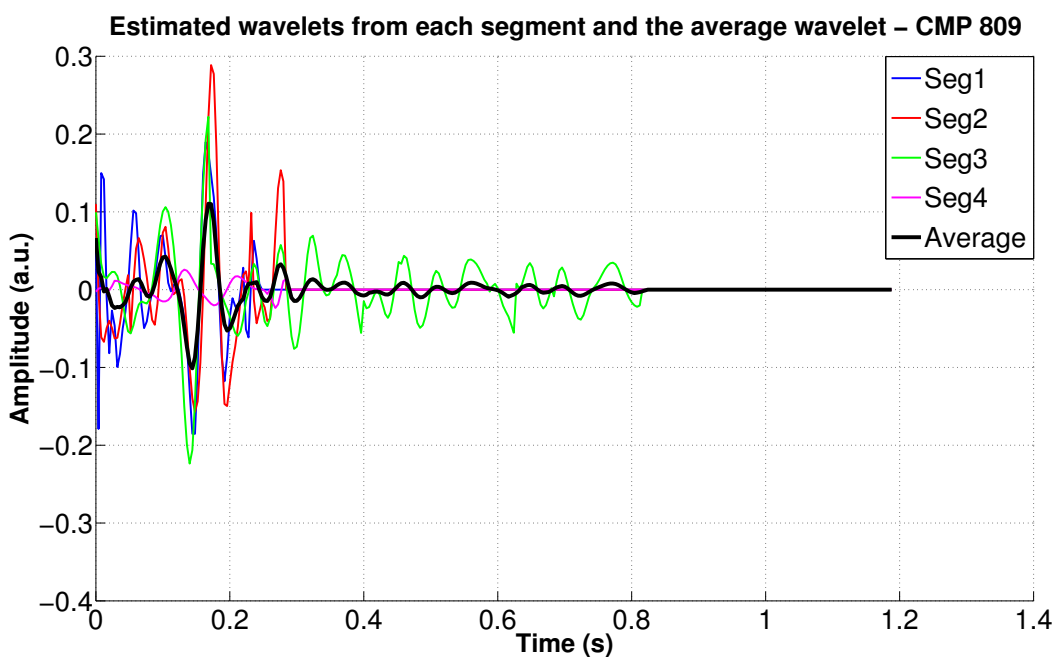
Source: From author.

Figure 38 – The average statistical wavelet estimated and the synthetic and real migrated seismic traces for the CMP 809. The correlation coefficient was 0.674.
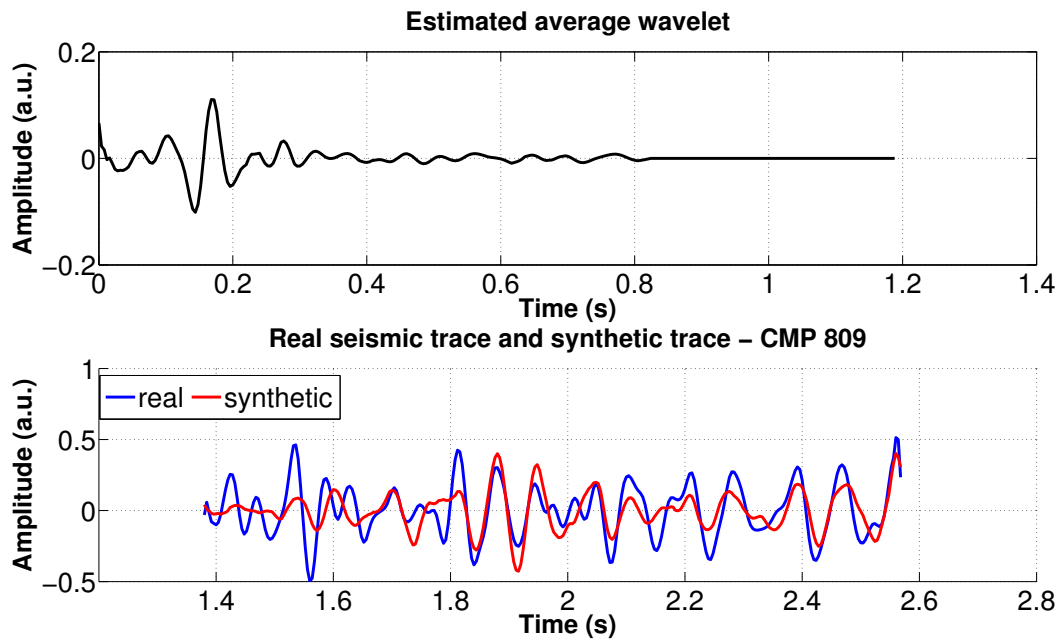
Source: From author.

the seismic wavelet are shown at Figures 39 and 40. The best match location for the well tie with deterministic approach using the migrated section was the same as the well tie made on the stacked section. The higher correlation coefficient between the synthetic and the real trace was on CMP 809, with a correlation coefficient of 0.712.

Figure 39 – Correlation Coefficient x CMPs for the Well A with a migrated seismic section through the deterministic method to estimate the wavelet. The best match location is also on CMP 809, but the correlation coefficient using the deterministic approach is higher than that of the statistical approach, it is 0.712.
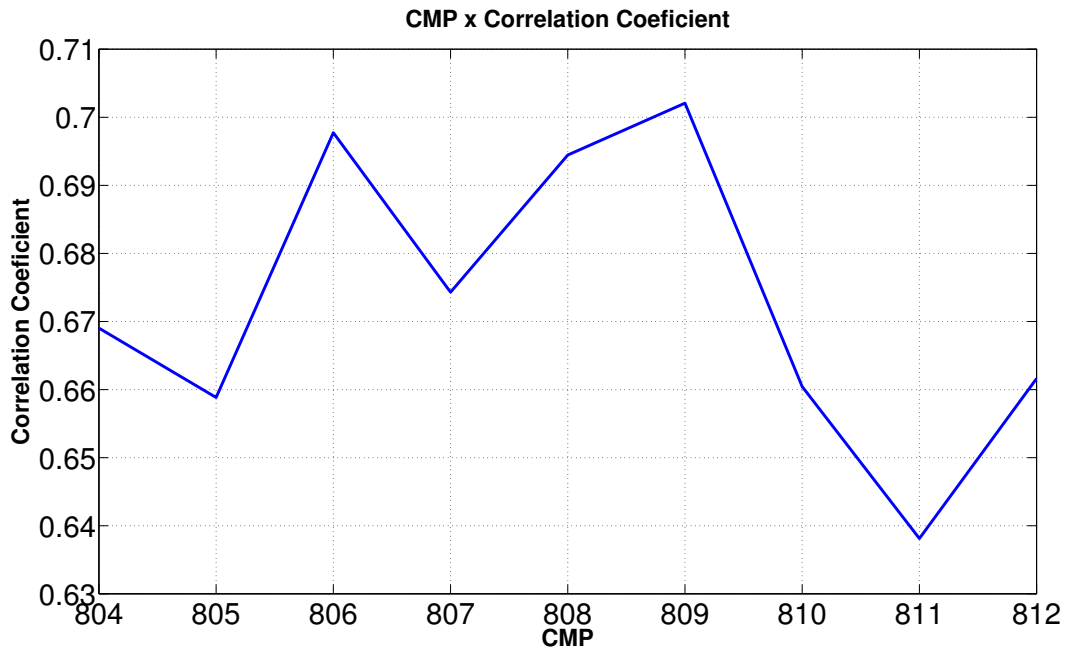
Source: From author.

Figure 40 – The wavelet estimated through the deterministic method and the synthetic and real migrated seismic trace on CMP 809. The correlation coefficient was 0.712.
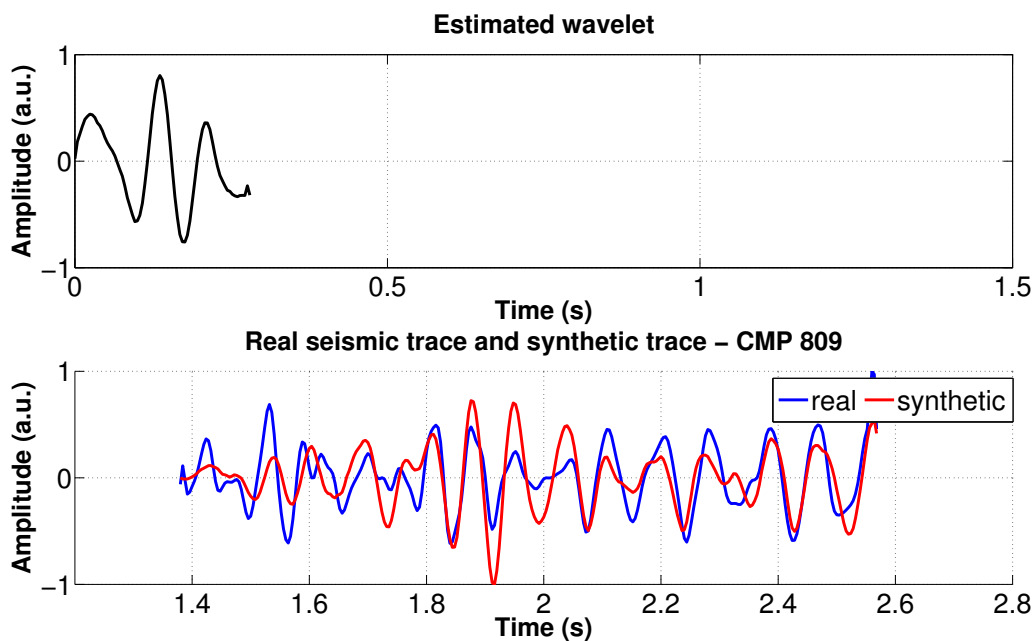
Source: From author.

4.6   Time migrated seismic section - Well B

Applying the statistical predictive deconvolution method to estimate the wavelet on the migrated seismic section along with informations of the well B yields to a best match location on CMP 1573, such as when using the stacked seismic section. The correlation coefficient of the tie through the statistical estimative of the wavelet on CMP 1573 was 0.741, and on CMP 1574, it was 0.728, as shown at Figures 41 and 42.

It was also performed the estimative of the average statistical wavelet for the well B on the migrated CMP 1573. The correlation coefficient in this case was slightly lower than the predictive deconvolution on one segment alone, as shown at Figures 43 and 44. For the average wavelet, the correlation coefficient of the well to seismic tie was 0.734, while the correlation coefficient of the tie when using the usual predictive deconvolution was 0.741 (see Figure 42).

The best match location for the well B with the migrated seismic section using the deterministic estimative of the wavelet was on CMP 1573 (see Figure 45), the same as when using the predictive estimative of the wavelet for the migrated section (see Figure 41) and the same for the results on the stacked seismic section (see Figures 28 and 32). Using the migrated seismic section and the deterministic estimative of the wavelet, it was obtained the best result on the quality of the well to seismic tie, a correlation of 0.811 between the real migrated seismic trace and the synthetic trace.

Figure 41 – (a) Correlation Coefficient x CMPs for the Well B with a migrated seismic section using the predictive deconvolution method to estimate the seismic wavelet. The best match location for the predictive estimative is on CMP 1573, with a correlation coefficient of 0.741. (b) Prediction lag x Correlation Coefficient for the CMP 1573 with a migrated seismic section. (c) Operator length x Correlation Coefficient for the CMP 1573 with a migrated seismic section.

(a)

(b)

(c)
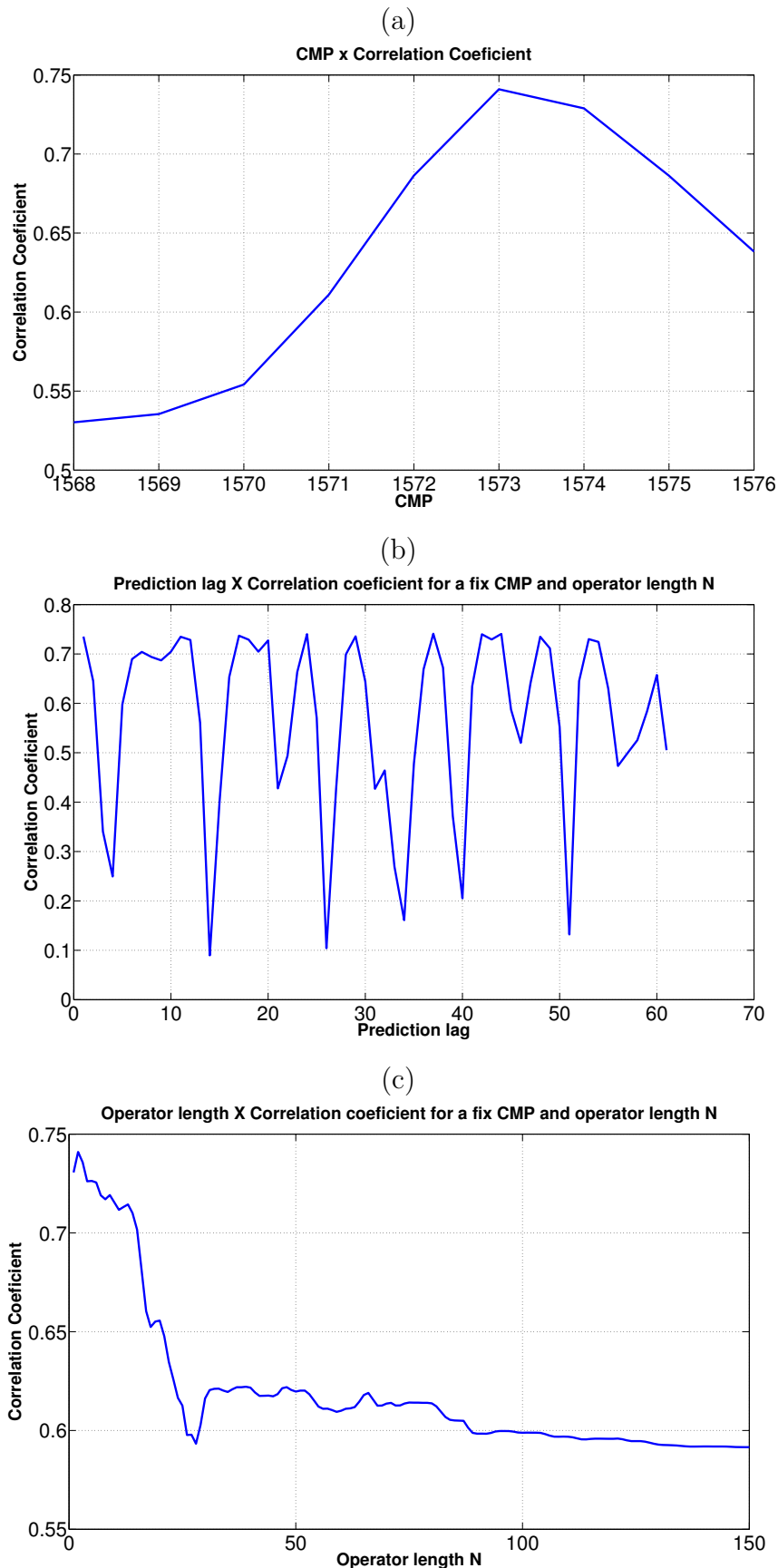
Figure 42 – The wavelet estimated through the statistical method and the synthetic and real
seismic trace from a migrated seismic section on CMP 1573. The correlation
coefficient was 0.741.
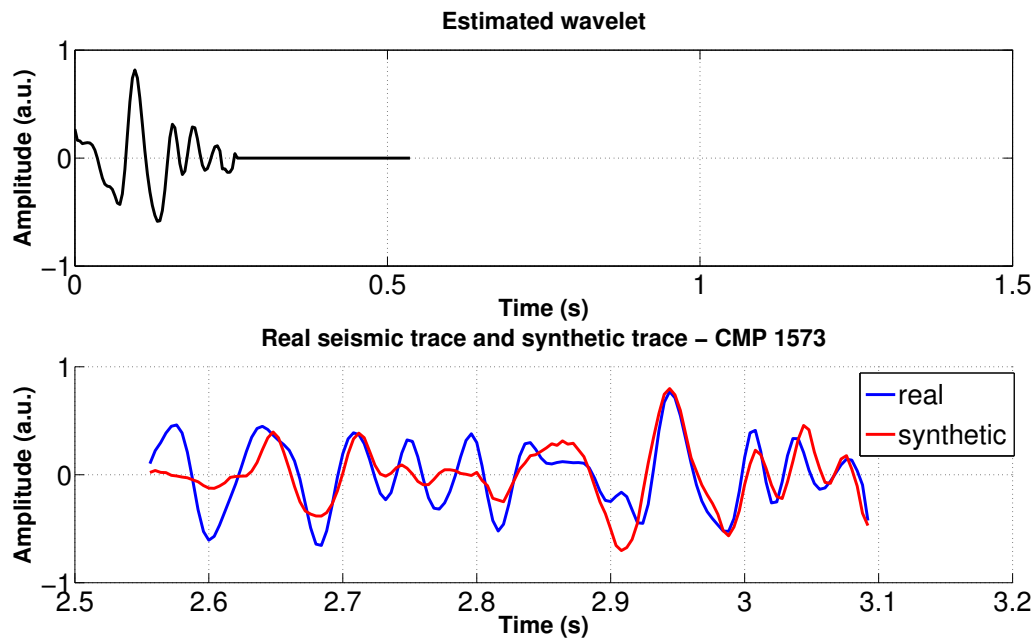
Source: From author.

Figure 43 – The wavelets estimated through the predictive deconvolution from each segment of
the migrated seismic trace and the average wavelet used to compute the synthetic
trace calculated through a migrated seismic section.
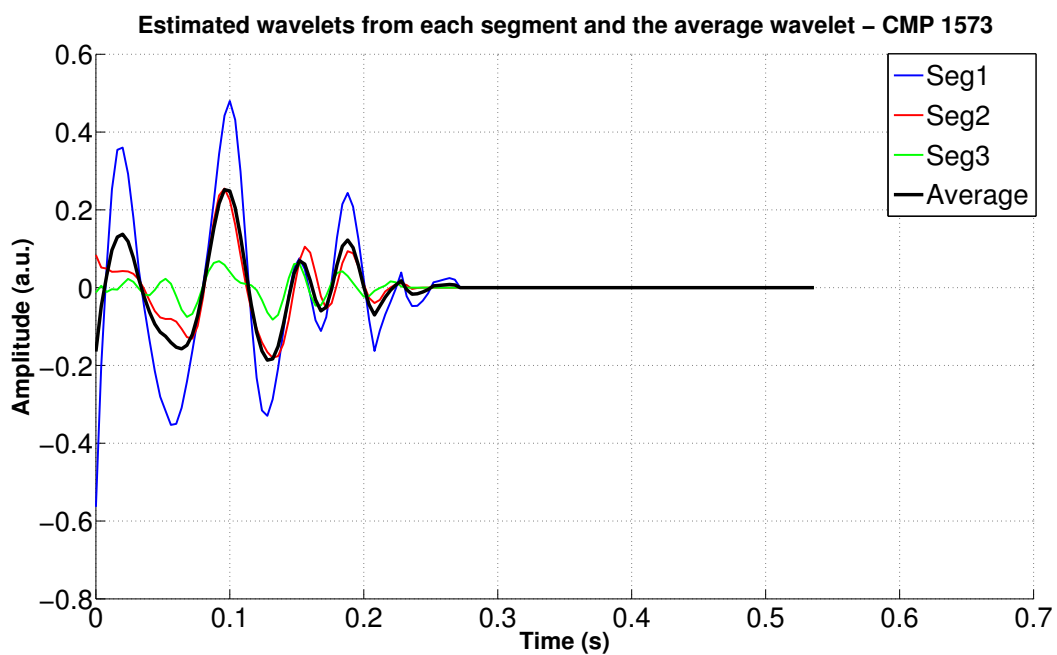
Source: From author.

Figure 44 – The average wavelet estimated and the synthetic and real seismic traces for the CMP 1573 from the migrated seismic section. The correlation coefficient is 0.734.
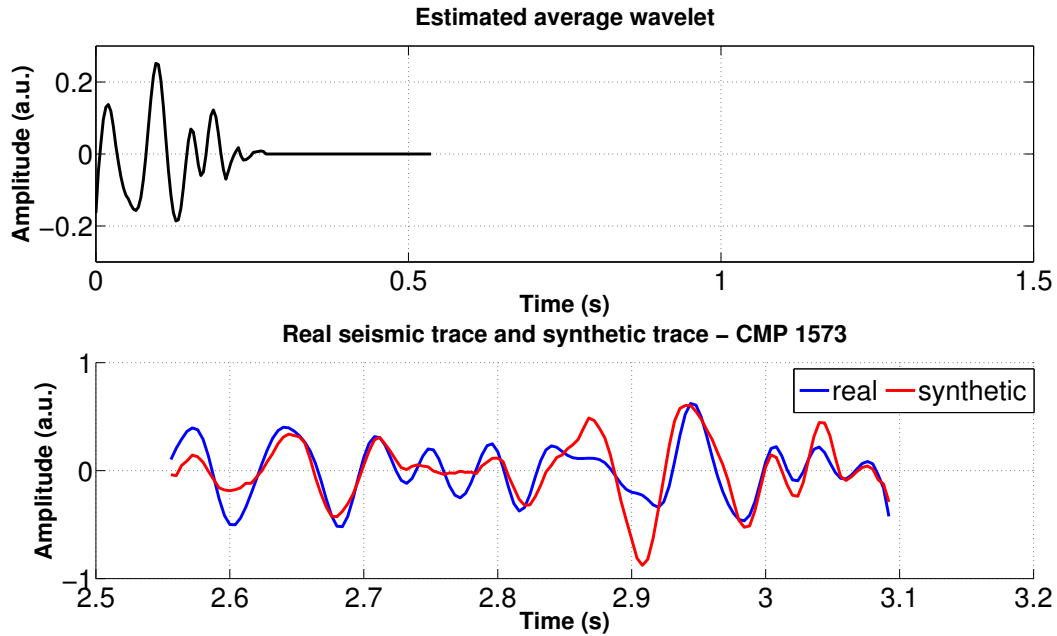
Source: From author.

Figure 45 – Correlation Coefficient x CMPs for the Well B with a migrated seismic section using the deterministic method to estimate the seismic wavelet. The best match location is on CMP 1573, with a correlation coefficient of 0.811.
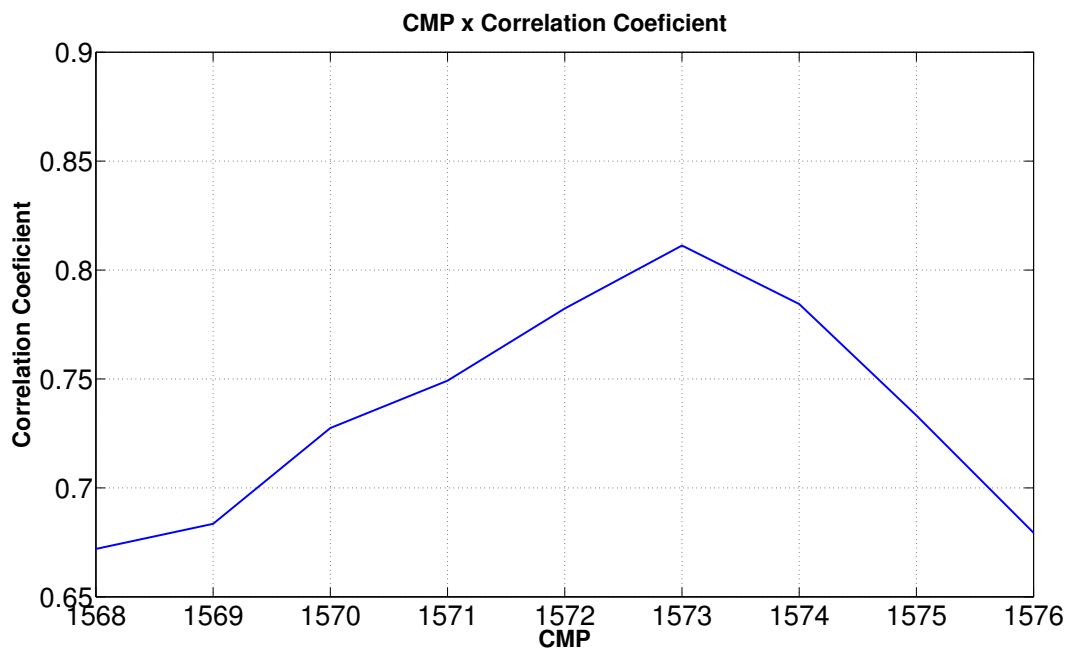
Source: From author.

Figure 46 – The wavelet estimated through the deterministic method and the synthetic and real seismic trace from the migrated seismic section on CMP 1573. The correlation coefficient of the well to seismic tie was 0.811.
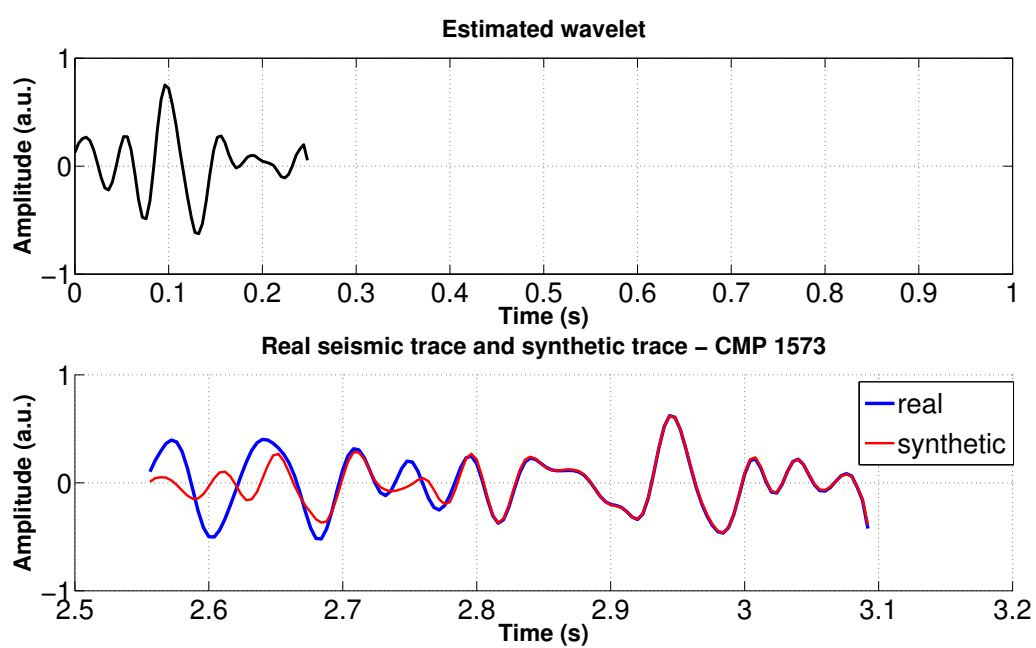
Source: From author.

5 DISCUSSION

As mentioned before, in this study we compared the well to seismic tie made with two different methods to estimate the wavelet. Beside that, we analyze that well geometry deviation can lead to a low correlation factor between synthetic and real seismic trace. In general, we relate the CMPs with the correlation coefficient of the tie, in order to find the best match location and also made connections between the correlation coefficient of the tie with the parameters of the predictive deconvolution.

Figures 22b, 35b, 28b, 41b showed the relations between the prediction lag of the predictive deconvolution with the correlation coefficient. As mentioned previously, the prediction lag is how much advanced in time the segment of the seismic trace will be when designing the desire output of the deconvolution. All the figures have the same pattern in view and it is related to the periodicity of the input trace. Figures 22c, 35c, 28c, 41c showed the relations between the operator length of the deconvolution with the correlation coefficient. Ideally, the longer the operator the best the resolution of the deconvolution. However, increasing operator length does not indefinitely improve the results because spurious spikes are introduced to the result. In fact, after a given length, the increase of the operator length does not improve the result of the deconvolution, as can be seen at the figures mentioned. In practice, the choice of the prediction lag and operator length that produces the best result of the predictive deconvolution is dictated by the signal-noise ratio.

As for the results on well A of the stacked seismic section, the best match location was the same for the both methods to estimate the wavelet, on CMP 809 (see Figure 22), very close to the posted well location, CMP 808. As different methods to estimate the wavelet leads to different wavelets, it is not uncommon for the best match location to be different with different approaches. It is expected that the average wavelet from the predictive deconvolution produces better results because it was computed from wavelets estimated from different segments of the seismic trace, therefore, its frequency content tends to be similar to that of the real seismic trace. The results on well A confirmed this supposing. The correlation coefficient increased from 0.635 (see Figure 23) to 0.653 (see Figure 25) when using the average wavelet on the stacked seismic section, and from 0.658 (see Figure 36) to 0.674 (see Figure 38) when using the migrated seismic section. As for the well B, the average estimated wavelet produced better results than the predictive deconvolution on one segment alone on the stacked seismic section. On CMP 1573, the correlation increased from 0.720 to 0.756 (see Figures 29 and 31) when using the average predictive wavelet on the stacked seismic section. However, on the migrated section, the average estimated wavelet produced a correlation coefficient slightly lower (correlation of

0.734) than the predictive deconvolution on one segment, correlation of 0.741 (see Figures 42 and 44).

The deterministic estimative of the wavelet tends to produce better results on the tie, once it is based on the well log data and on the seismic data. However, the need to use both well logs and seismic data in corresponding scales, makes it more sensitive to errors on the time-depth relationship. For both well logs and both seismic sections, the deterministic estimative of the wavelet lead to better results on the tie, as can be seen in Figures27, 40, 34, 46.

As for the use of a stacked seismic section and a migrated seismic section, it is expected that a migrated section with good quality leads to better results on the estimative of the wavelet, once it eases the diffraction and reposition the reflectors. Almost all the results were better on the migrated seismic section, the only exception was the deterministic estimative on well A, that was slightly better on the stacked section 27, with correlation of 0.727, than on the migrated section 40, with a correlation of 0.712.

Frequency attenuation caused by the intrinsic attenuation in rocks causes loss of high frequencies in the propagating waveform with increasing travel-time. This gives rise to a nonstationary behavior in the shape of the wavelets associated with reflection events at different times. The wavelet estimated from both methods are considered to be stationary, therefore, it may be a factor that contribute to decrease the correlation coefficient of the results. Moreover, the real data used is characterized by faults and fractures, since it is a host-graben structure, which contributes even more to the frequency attenuation.

Analyzing the results, it is possible to note that the correlation coefficient between the seismic trace and the synthetic for the well A is lower than for the well B. A possible cause for that difference is because of acquisition problems on the well A (KEYS, 1998). To solve that problem, a VSP from a nearby well was substituted for the well A vertical seismic profile. This may affect the time-depth relationship for this well, which causes the estimated wavelet, specially for the deterministic method, to do not be as accurate as it could be and consequently the correlation coefficient is not as high as it could.

According to Keys (1998) and Madiba e McMechan (2003) along the well A, a unconformity occurs at the base of the Cretaceous, at 1.97 s, separating rocks from the Tertiary and from the Jurassic. This event is visible on the synthetic trace for the well A. The probable causes for the unconformity do not standout on the real seismic trace, are the attenuation and absorption effects of the propagating wave with depth, once the seismic do not have as much vertical resolution as the synthetic trace that have excellent vertical resolution. In Gleinnie e Parsely (1986) has a stratigraphic column for northern North Sea reservoir rocks which shows the main features of rock reservoir. Figures 47, 48 and 49 show a possible lithological interpretation for the wells A and B based on the information provided by Gleinnie e Parsely (1986), Keys (1998), Madiba e McMechan

(2003) and the gamma ray log on the time axis. The heavily faulted upper Jurassic formations (KYRKJEBO R.; FALEIDE, 2004) begins just below the BCU unconformity in well A at approximately 1.97 s and in well B at approximately 2.55 s. Therefore, due to the structural characteristics of this formation, it is not expected a high quality on the well to seismic tie. The well B does not contain Tertiary formations once it begins below the BCU.

Other important point which must be taken into account, are the results of the well to seismic tie through the correlation coefficient using different segments of the trace. The Figures 50a and 50b shows the well to seismic tie for the well A with the migrated seismic section, with the values of the correlation coefficient of different segments of the trace. The tie of the Figure 50a was made with the deterministic estimation of the wavelet, and the tie of the Figure 50b was made with the average predictive estimation of the wavelet. In both of them the correlation coefficient of the initial parts of the trace is very low and it gets higher with time.

Figures 51a) and b) shows the well tie for the well B with the migrated seismic section and the estimated wavelets through the deterministic approach and through the predictive approach. The correlation coefficient of the initial parts of the trace is also lower than the final parts, such as the tie for the well A. To understand the possible reason for that difference on the quality of the well tie in different segments of the trace, we analyze the tie together with the gamma ray log and the caliper log. The gamma ray log is a indicator of the shale content on the formation and the caliper log describe the diameter of the borehole along its depth during the drilling. The measurements that are recorded can be an important indicator of cave ins or shale swelling in the borehole, which can affect the results of the sonic and density logs. Performing this analyze, we chose the best tie for the well A and the best tie for the well B.

Figure 52a show that the segment with the lower correlation coefficient $c_1 = 0.409$ corresponds to the zone where the caliper log is unstable, which directly affects the sonic and density measurements and, consequently, directly affects the quality of the well to seismic tie. Keys (1998) mentioned on their article about the Viking Graben data set problems during the acquisition of data along the well A, which might be related with this anomalous zone on the caliper log. This first segment is related with the lithology of the formation above the Cretaceous unconformity at 1.97 s. The Paleocene and Cretaceous rocks above the unconformity are deep water clastic sediments and as they are deposited in a slope in the basin, the formation contain turbidites. On the second $c_2 = 0.805$ and third segment $c_3 = 0.839$, it is possible to note that when the caliper log gets more stable, the correlation increases although the shale content also increases due to the Jurassic rocks associated with deepwater shales.

In Figure 53, it is shown the relations between the gamma ray log, the caliper

Figure 47 – A possible lithological interpretation for the well A based on the gamma ray logs. Formations from the Tertiary and Jurassic are present.

Source: From the author.

Figure 48 – A possible lithological interpretation for the well B based on the gamma ray logs. Since it begins below the BCU, it contains only Jurassic formations.
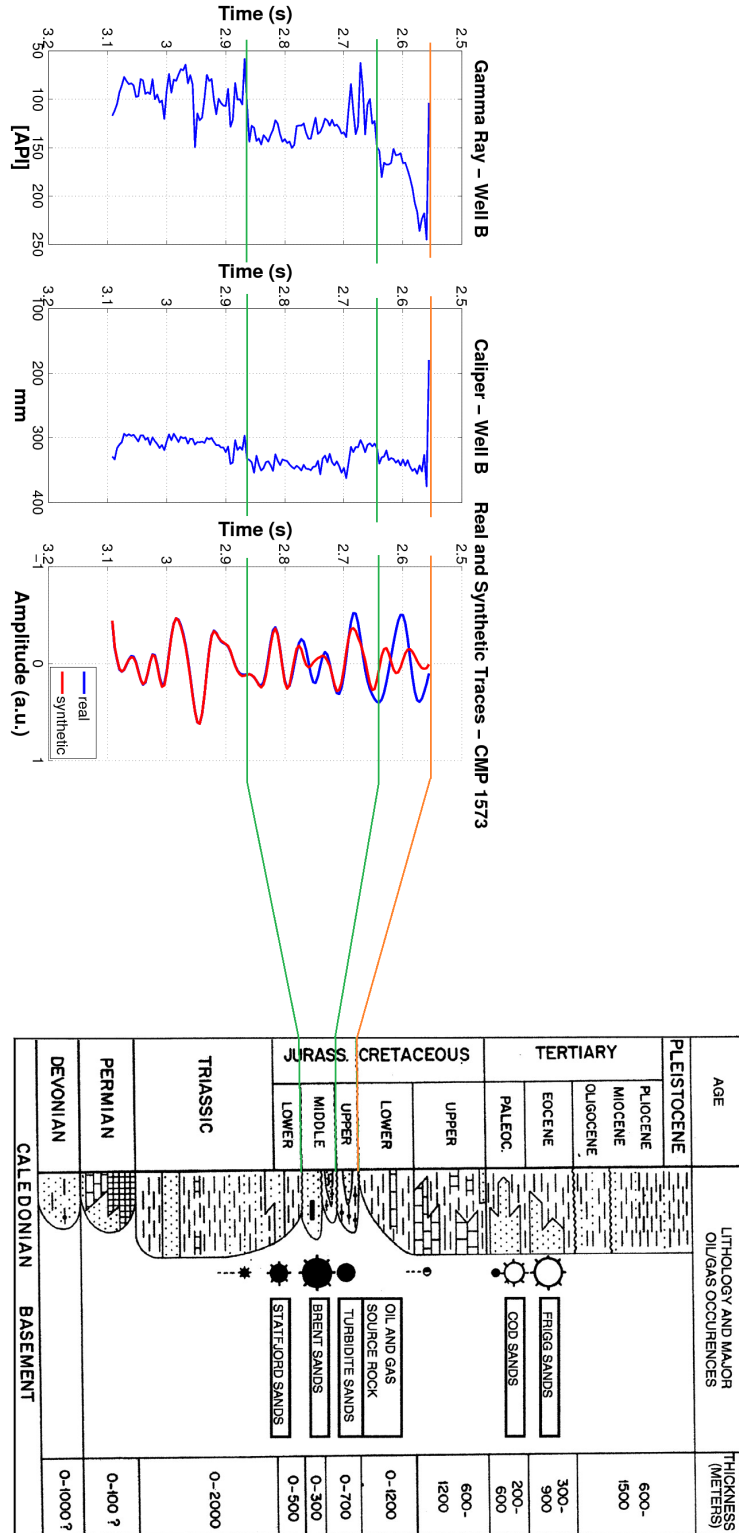
Source: From the author.

Figure 49 – The lithological interpretations of the well A and the well B together with the stratigraphic column. As the sediments are deposited in a slope into the basin, the BCU appear at different times on the gamma ray log of the well A and of the well B.
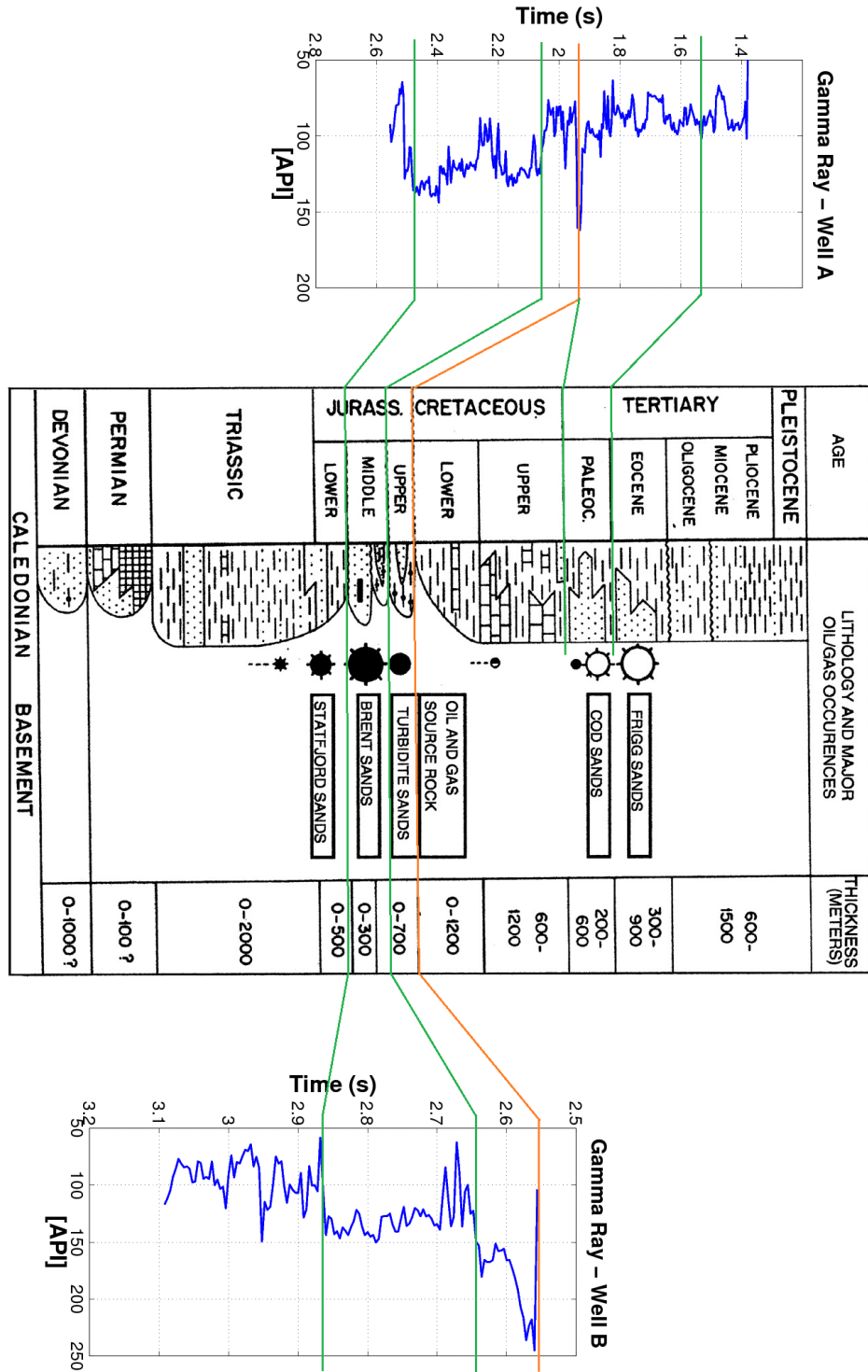
Source: From the author.

Figure 50 – Well tie for the well A with a migrated seismic section using the average predictive estimated wavelet. Well tie for the well A with a migrated seismic section using the deterministic estimated wavelet
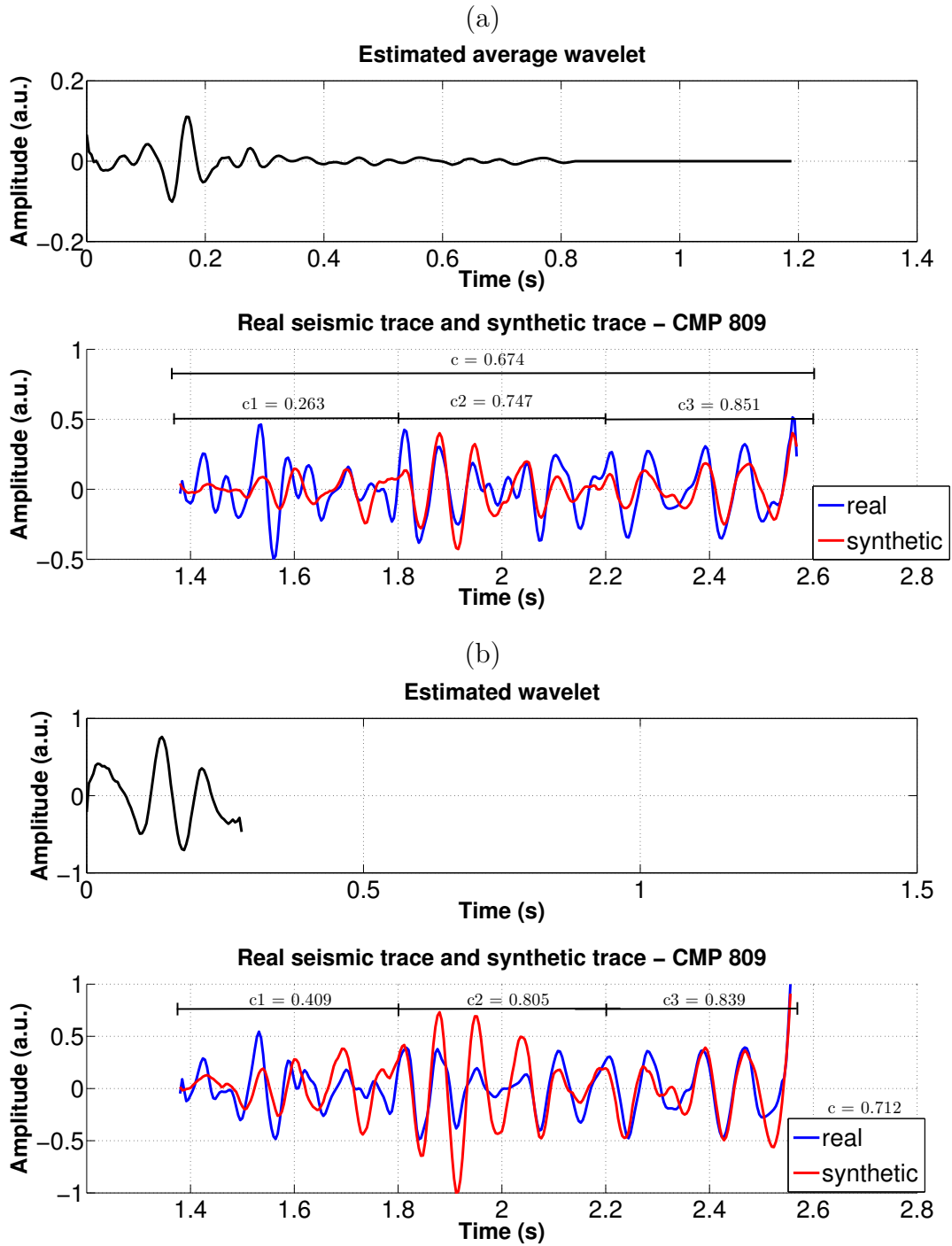
Source: From author.

Figure 51 – Well tie for the well B with a migrated seismic section and the predictive esti-
mated wavelet. b) Well tie for the well B with a migrated seismic section and the
deterministic estimated wavelet.

(a)

(b)
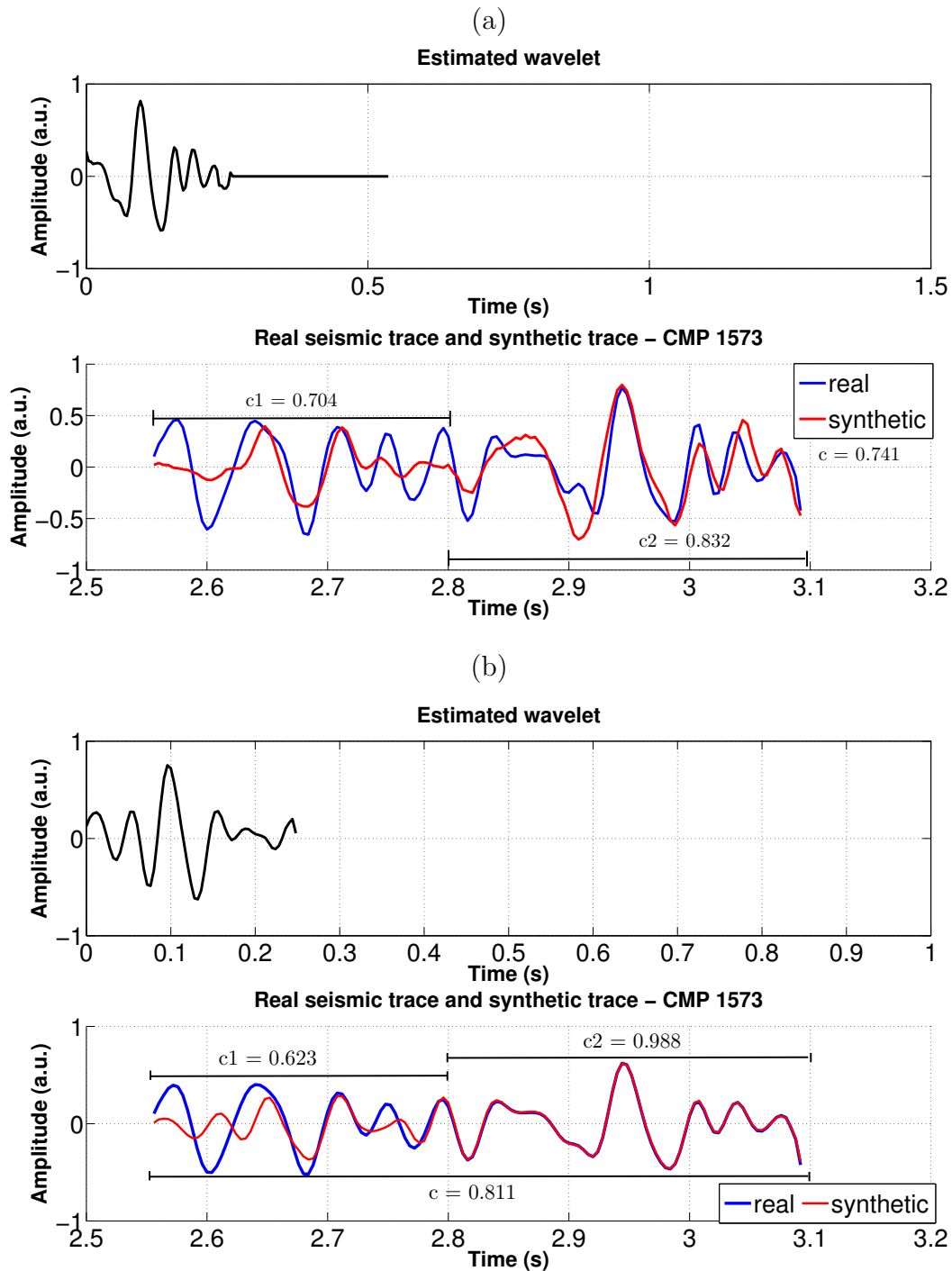
Source: From author.

Figure 52 – Well tie for the well A with the migrated seismic section and the deterministic estimated wavelet and the gamma ray and caliper logs.
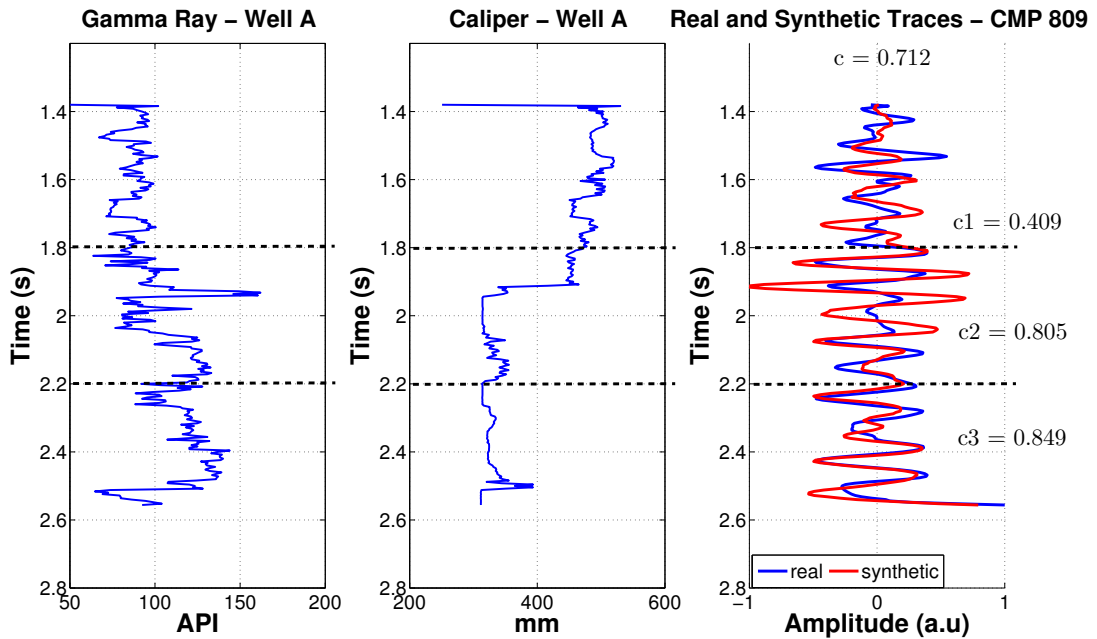
Source: From author.

log and the well to seismic tie for the well B. As the Paleocene and Cretaceous rocks are deposited in a slope in the basin, the Cretaceous unconformity that on well A is at approximately 1.97 s, on well B it is approximately at 2.4 s, so the beginning of the synthetic trace for the well B is just below the unconformity. Therefore, it covers the Jurassic rocks. For this well, although the caliper log is relatively stable along the hole trace, the first segment of the trace shows a lower correlation coefficient. This might be due to the faults associated with the Cretaceous unconformity that constitute the oil and gas traps and the deep water shales associated with it, as mentioned by Madiba e McMechan (2003) and as can be seen by the gamma ray log. As the shale content tends to decrease and the caliper log gets stable, the quality of the well tie increases and the excellent result of a correlation of $c_2 = 0.988$ for the second part of the trace was obtained.

Figure 53 – Well tie for the well B with the migrated seismic section and the deterministic estimated wavelet and the gamma ray and caliper logs.
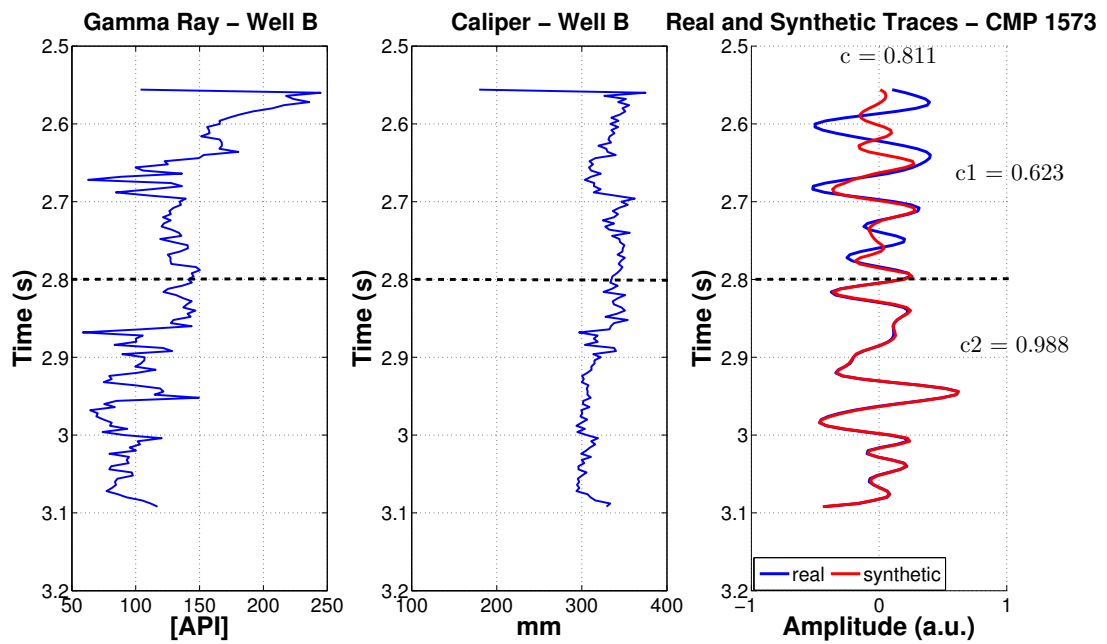
Source: From author.

6 CONCLUSIONS

In this study we compare the quality of the well to seismic tie made from two different algorithms to estimate the wavelet (the semi automatic deterministic and statistical estimative). The application on the synthetic data shows that both methods were satisfactory on the seismic wavelet estimative. In the case of the synthetic examples, this is confirmed by high values of correlation coefficient which reached values higher than 0.90.

On the real Viking Graben data set, the predictive estimation, based on the classical assumptions of the convolutional model produced a good estimative on the well to seismic tie for both wells. All of them with a correlation above 0.60. Moreover, the predictive estimation through the average predictive estimated wavelet showed slightly improved results on the quality of the tie. The deterministic estimation of the wavelet produced the better results, although it is not as good as it could be on the well A because of issues on the time-depth relationship. On well A, the correlation was of 0.712 and on well B the correlation was of 0.811.

The influence of the shale content and the stability of the diameter of the borehole during acquisition was analyzed and the caliper logs showed the anomalies that can directly affects the quality of the well to seismic tie and consequently, the estimated wavelet. It was also possible to relate the lithology of the formations with the results of the tie. This analysis involving the caliper log, can be an indicative for an estimated wavelet using segments of traces instead of the entire trace, providing a better correlation between the well and the seismic (for both methods of estimative). Zones with faults and increasing shale content also showed to be possible artifacts that cant affects the quality of the well tie.

Because of the acquisition problems on the well A, the time-depth relationship was compromised. It would be interest to try more accurate statistical methods to estimate the wavelet for this well, such as the homomorphic deconvolution, that does not imply a minimum phase wavelet and a white reflectivity. Moreover, try to recover the zones of the sonic and density logs affected by problems related with the stability of the diameter of the borehole, would be interest to calculate a new reflectivity series free from those effects and, hopefully, obtain an even better quality on the well to seismic tie.

Bibliography

BULAND, A.; OMRE, H. Bayesian wavelet estimation from seismic and well data. *Geophysics*, v. 68, n. 6, p. 2000–2009, nov. 2003. Disponível em: <http://library.seg.org/doi/abs/10.1190/1.1635053>.

EDGAR, J.; BAAN, M. van der. How reliable is statistical wavelet estimation? *Geophysics*, v. 76, n. 4, p. V59–V68, 2011. Disponível em: <http://library.seg.org/doi/abs/10.1190/1.3587220>.

GARDNER, G. H. F. Formation velocity and density -the diagnostic basics for stratigraphic traps. *Geophysics*, v. 39, p. 770, 1974.

GLEINNIE, K. W.; PARSELY, J. A. Introduction to the petroleum geology of the North Sea. *Blackwell Science Inc*, 1986.

KEYS, R. G. *Comparison of seismic inversion methods on a single real data set, open file publications.* Tulsa, OK: Society of Exploration, 1998.

KING, F. W. *Hilbert transforms.* Cambridge Eng.; New York: Cambridge University Press, 2010. v. 2.

KYRKJEBO R., R. H.; FALEIDE, J. I. Unconformities related to the Jurassic–Cretaceous synrift–post-rift transition of the northern North Sea. *Journal of the Geological Society*, v. 161, p. 1–17, jan. 2004.

LUNDSGAARD, A. K.; KLEMM, H.; CHERRETT, A. J. Joint bayesian wavelet and well-path estimation in the impedance domain. *Geophysics*, n. 2, p. M15–M31, mar. 2015.

MA ROY E. WHITE, T.-Y. H. H.-D. Wavelet estimation by matching well-log, vsp, and surface-seismic data. *Geophysics*, v. 7, n. 4, p. 384–391, dez. 2010.

MADIBA, G. B.; MCMECHAN, G. A. Processing, inversion, and interpretation of a 2d seismic data set from the North Viking Graben, North Sea. *Geophysics*, v. 68, n. 3, p. 837–848, maio 2003. Disponível em: <http://geophysics.geoscienceworld.org/content/68/3/837>.

MONROE, J.; FIGUEIREDO, J. de. Seismic attributes analysis for the identification and characteruzation of hydrocarbon reservoirs - revisiting the viking graben dataset. *14th International Congress of the Brazilian Geophysical Society*, v. 39, p. 893–897, 2015.

OLDENBURG, D.; LEVY, S.; WHITTALL, K. Wavelet estimation and deconvolution. *Geophysics*, v. 46, n. 11, p. 1528–1542, nov. 1981. Disponível em: <http://library.seg.org/doi/abs/10.1190/1.1441159>.

ROBINSON, E. Predictive decomposition of time series with application to seismic exploration. *Geophysics*, v. 32, n. 3, p. 418–484, 1967. Disponível em: <http://library.seg.org/doi/abs/10.1190/1.1439873>.

ROBINSON, E. A. Predictive decomposition of seismic traces. *Geophysics*, v. 22, n. 4, p. 767–778, 1957.

ROBINSON, S. T. E. A. *Digital imaging and deconvolution: the ABCs of seismic exploration and processing.* [S.l.]: SEG Books, 2008.

SIMM, M. B. R. *Seismic amplitude: an interpreter's handbook.* [S.l.]: Cambridge University Press, 2014.

WHITE, R. Partial coherence matching of synthetic seismograms with seismic traces. *Geophysical Prospecting*, v. 28, n. 3, p. 333–358, 1980.

WHITE, R. Tying well-log synthetic seismograms to seismic data: the key factors. In: *SEG technical program expanded abstracts.* [S.l.]: Society of Exploration Geophysicists, 2003, (SEG Technical Program Expanded Abstracts). p. 2449–2452.

WHITE, R.; SIMM, R.; XU, S. Well tie, fluid substitution and AVO modelling: a North Sea example. *Geophysical Prospecting*, v. 46, n. 3, p. 323–346, maio 1998.

WHITE, R. E.; O'BRIEN, P. N. S. Estimation of the primary seismic pulse. *Geophysical Prospecting*, v. 22, n. 4, p. 627–651, 1974.

WHITE, R. E.; SIMM, R. Tutorial: good practice in well ties. *First Break*, v. 21, n. 10, 2013.

YILMAZ, O. *Seismic data analysis: processing, inversion, and interpretation of seismic data.* [S.l.]: SEG Books, 2000.

APPENDIX

APPENDIX A – Optimum Wiener Filters

The following discussion of optimum Wiener filters is based on (YILMAZ, 2000). The Wiener filtering is optimum at the least squares sense. In other words, it involves the designing of a filter $f(t)$ so that the least squares error between the actual and the desired output is minimum. The error L is defined as:

$$L = \sum_t (d_t - y_t)^2, \tag{A.1}$$

where d_t is the desired output of the filtering process and y_t is the actual output. The actual output is the convolution of the filter f_t with the input x_t:

$$y_t = f_t * x_t = f_\tau x_{t-\tau} \tag{A.2}$$

Substituting equation A.2 into equation A.1, it gives

$$L = \sum_t (d_t - \sum_\tau f_\tau x_{t-\tau})^2 \tag{A.3}$$

Expanding the square term

$$L = \sum_t \left[d_t^2 - 2d_t \sum_\tau f_\tau x_{t-\tau} + (\sum_\tau (f_\tau x_{t-\tau}))^2 \right] \tag{A.4}$$

$$L = \sum_t d_t^2 - 2\sum_t d_t \sum_\tau f_\tau x_{t-\tau} + \sum_t (\sum_\tau f_\tau x_{t-\tau})^2 \tag{A.5}$$

As the goal is to find the filter coefficients $(f_0, f_1, f_2, ..., f_{n-1})$ so that the error L is minimum, the variation of L with respect to f_i is set to zero:

$$\frac{\partial L}{\partial f_i} = 0, i = 0, 1, 2, 3, \cdots, (n-1) \tag{A.6}$$

$$\frac{\partial L}{\partial f_i} = -2\sum_t d_t x_{t-i} + 2\sum_t (\sum_\tau f_\tau x_{t-\tau}) x_{t-i} = 0 \tag{A.7}$$

$$\sum_t d_t x_{t-i} = \sum_t (\sum_\tau f_\tau x_{t-\tau}) x_{t-i} \tag{A.8}$$

$$\sum_t d_t x_{t-i} = \sum_t x_{t-i} \sum_t x_{t-\tau} \sum_\tau f_\tau \tag{A.9}$$

$$\sum_t x_{t-\tau} x_{t-i} \sum_\tau f_\tau = \sum_t d_t x_{t-i} \tag{A.10}$$

By writing

$$\sum_t x_{t-\tau} x_{t-i} = r_{i-\tau}, \tag{A.11}$$

and

$$\sum_t d_t x_{t-i} = g_i \tag{A.12}$$

and substituting those relations on equation A.10, it gives

$$\sum_\tau r_{i-\tau} f_\tau = g_i \tag{A.13}$$

Putting equation A.13 into matrix form, it leads to

$$\begin{pmatrix} r_0 & r_1 & r_2 & \cdots & r_{n-1} \\ r_1 & r_0 & r_1 & \cdots & r_{n-2} \\ r_2 & r_1 & r_0 & \cdots & r_{n-3} \\ \vdots & \vdots & \vdots & \ddots & \vdots \\ r_{n-1} & r_{n-2} & r_{n-3} & \cdots & r_0 \end{pmatrix} \begin{pmatrix} f_0 \\ f_1 \\ f_2 \\ \vdots \\ f_{n-1} \end{pmatrix} = \begin{pmatrix} g_0 \\ g_1 \\ g_2 \\ \vdots \\ g_{n-1} \end{pmatrix} \tag{A.14}$$

Equation A.14 configures the normal Wiener equations, where r_i are the autocorrelation lags of the input and g_i are the lags of the crosscorrelation between the desired output and the input. Since the autocorrelation matrix is Toeplitz, the optimum Wiener filter coefficients f_i can be computed by Levinson recursion.

The Wiener filter applies to a large class of problems in which any desired output can be considered. The deconvolution problems can be classified according to the desired output d_t considered.

A.1 Spiking Deconvolution

If the desired output of the filtering processing is set to be a zero-delay spike, d_t is $d_t : (1, 0, 0, ...n - 1)$. Computing the crosscorrelation between the desired output and the input series according to equation A.12, the normal Wiener equation A.14 for the case of the spiking deconvolution takes the form

$$
\begin{pmatrix}
r_0 & r_1 & r_2 & \cdots & r_{n-1} \\
r_1 & r_0 & r_1 & \cdots & r_{n-2} \\
r_2 & r_1 & r_0 & \cdots & r_{n-3} \\
\vdots & \vdots & \vdots & \ddots & \vdots \\
r_{n-1} & r_{n-2} & r_{n-3} & \cdots & r_0
\end{pmatrix}
\begin{pmatrix}
f_0 \\
f_1 \\
f_2 \\
\vdots \\
f_{n-1}
\end{pmatrix}
=
\begin{pmatrix}
x_0 \\
0 \\
0 \\
\vdots \\
0
\end{pmatrix}
\tag{A.15}
$$

A.2 Predictive Deconvolution

To find the normal Wiener equation for the case of the predictive deconvolution, it is necessary to set the desired output. In this case, the desired output is a time advanced form of the input signal. If the input signal is $x(t)$, the desired output is $d_t = x(t+\alpha)$. To desing a filter that predicts $x(t + \alpha)$ from $x(t)$, it is necessary to compute the crosscorrelation between the desired output $x(t + \alpha)$ with the input signal $x(t)$. According to equation A.12, the crosscorrelation for this case will be

$$
g_\tau = \sum_t d_t x_{t-\tau} = \sum_t x_{t+\alpha} x_{t-\tau} = \sum_t x_t x_{t-(\alpha+\tau)}.
\tag{A.16}
$$

Since

$$
r_\tau = \sum_t x_t x_{t-\tau}
\tag{A.17}
$$

For the $\alpha + \tau$ lag as in equation A.16, equation A.17 becomes

$$
r_{\alpha+\tau} = \sum_t x_t x_{t-(\alpha+\tau)} = g_\tau.
\tag{A.18}
$$

Substituting this result on the general normal Wiener equations A.14, the normal equations that must be solved to find the prediction filter $(f_0, f_1, f_2, f_3...)$ is set. In this case, note that to find the prediction filter, it is only needed the input signal.

$$
\begin{pmatrix}
r_0 & r_1 & r_2 & \cdots & r_{n-1} \\
r_1 & r_0 & r_1 & \cdots & r_{n-2} \\
r_2 & r_1 & r_0 & \cdots & r_{n-3} \\
\vdots & \vdots & \vdots & \ddots & \vdots \\
r_{n-1} & r_{n-2} & r_{n-3} & \cdots & r_0
\end{pmatrix}
\begin{pmatrix}
f_0 \\
f_1 \\
f_2 \\
\vdots \\
f_{n-1}
\end{pmatrix}
=
\begin{pmatrix}
r_\alpha \\
r_{\alpha+1} \\
r_{\alpha+2} \\
\vdots \\
r_{\alpha+n-1}
\end{pmatrix}
\qquad (A.19)
$$